

REMARKS

I. Status of the Claims

Claims 1-29 were pending. The Examiner has made the Restriction Requirement, including the "additional election" requirement, final and withdrawn claims 11-29 from consideration under 37 C.F.R. § 1.142(b) as being drawn to non-elected inventions. Office action page 3. The Examiner states that claims 1-10 together with the elected Type VI FACIT and decorin are under examination to the extent that they are drawn to the elected invention. *Id.* Claims 1-10 have been rejected under 35 U.S.C. § 112, second paragraph. Office action pages 4-5.

With this Amendment, Applicants cancel non-elected claims 11-29. Applicants also amend independent claim 1 to recite the elected invention wherein the FACIT is Type VI collagen and the SLRP is decorin, and cancel claims 6 and 7 which recited the Markush groups of FACITs and SLRPs for use in the method of claim 1. Applicants reserve the right to file one or more divisional applications for the non-elected subject matter. Because the Examiner required restriction rather than a species election with respect to the Markush members of original claims 6 and 7, Applicants understand that each composition used in the method of claim 1 has been treated by the Office as a separate invention which may be prosecuted in one or more divisional applications.

Claims 1, 2, 4, 8, and 9 have been amended to clarify the claims and to limit the claims to the elected invention. These amendments are supported throughout the specification and original claims. In particular, claims 1 and 9 have been amended to correct informalities objected to by the Examiner, to clarify the nature of the stabilizing agent, and to limit the claims to the elected invention. These amendments are

supported throughout the specification and original claims. For example, pages 13-14 of the specification describe the general method for maintaining a desired shape of corneal tissues following an orthokeratological procedure. Page 7 of the specification, original claims 6 and 7, and the working examples each support that type VI collagen is a FACIT and that decorin is a SLRP for use in the methods of the invention. Claim 2 has been amended to clarify that “a patient” is the patient of claim 1. Claim 4 has been amended to clarify that it is the diameter of the fibril that is controlled by the stabilizing agent, as supported in original claim 4 and in the specification on page 14, first full paragraph. Claim 8 has been amended to clarify the antecedent basis, as supported in the original claim and in the specification on, for example, page 13 at the second full paragraph. Claim 9 has been amended to address the Examiner’s objection to “the step of a.” by deleting this recitation. Claim 9 has also been amended to clarify the nature of the stabilizing agent, as supported, for example, in Example 4 on pages 17-20.

II. Amendments to the Specification

The Examiner objected to the specification in several locations for failing to provide the full name of a technical term before using an abbreviation. The terms are sufficiently well-known in the art that they should not require further explanation. Nevertheless, in order to expedite prosecution, Applicants have amended the specification as requested by the Examiner in all locations where the term was not defined. For each of these amendments, Applicants provide evidentiary references to support that the abbreviations in the specification had an art-recognized meaning at the time the application was filed. For example, van der Rest et al. (J. Biol. Chem. Vol. 260,

pp. 220-225 (1985)) establishes in Figure 6 that “NC3” was an art-recognized abbreviation for the third noncollagenous domain of collagen. Lee et al. (Proc. Natl. Acad. Sci. U.S.A. Vol. 88, pp. 2768-2772 (1991)) provide in their “Abbreviations” section on page 2768 the abbreviations for basic fibroblast growth factor and glycosaminoglycan. Likewise, Sukurai et al. (Proc. Natl. Acad. Sci. U.S.A. Vol. 94, pp. 6279-6284 (1997)) provide the standard abbreviations for epidermal growth factor and transforming growth factor in the “Abbreviations” section on page 6279. The recognized abbreviation for transmission electron microscopy is provided in the Abstract of Al-Ghoul et al. (Mol. Vision Vol. 5, pp. 6-12 (1999)).

Applicants submit that an amendment to the specification to disclose the full name for a term originally presented by an art-recognized abbreviation, particularly given the context of the abbreviation, does not introduce new matter into the specification.

III. Objection to the Declaration

The Examiner states that the declaration is defective because Inventor Bruce H. DeWoolfson appears not to indicate whether he is a US citizen.

Applicants note the Declaration provides a box labeled “Citizenship” in which “US” is typed for both Inventor DeWoolfson and Inventor DeVore. The typed “US” in the Citizenship box is sufficient to indicate the citizenship of the inventor as required by 35 U.S.C. § 25, 37 C.F.R. § 1.63, and M.P.E.P. § 602. The typed indication of U.S. citizenship is consistent with the typed entry of other data on the Declaration. If after reviewing the Declaration the Examiner intends to maintain his objection, he is requested to contact the undersigned prior to issuing another Office action.

IV. Objections to the Specification

The Examiner has objected to the specification at several locations for failure to provide the full technical term prior to use of an art-recognized abbreviation. Office action page 4. The Examiner has also required an Abstract on a separate sheet. *Id.*

Applicants have amended the specification to ensure that the full term is provided before the first use of the noted abbreviations. As detailed in the discussion of the amendments in Section II, these amendments do not add new matter. Applicants note that the first occurrence of “BM” is defined on page 10 in the last sentence of the second full paragraph. Applicants, therefore, have not amended the second occurrence of “BM” pointed to by the Examiner. A new Abstract has been provided as an attachment to this Response, as requested by the Examiner, and a request that the new Abstract be entered included in the Amendments to the Specification section of this Response. Applicants believe the Examiner’s objections have each been addressed and request their withdrawal.

VI. Objection to the Claims

The Examiner objects to claims 1 and 9 and requests that the “a.” before “administering to...” be deleted. Office action page 4. Applicants have complied with the Examiner’s request and therefore ask that the objection be withdrawn.

VII. Rejections under 35 U.S.C. § 112, second paragraph

The Examiner rejects claims 1-10 under 35 U.S.C. § 112, second paragraph for failure to particularly point out and distinctly claim the subject matter Applicant regards as the invention. Office action page 4. The Examiner rejects independent claims 1 and

9 as indefinite because it is unclear whether the stabilizing agent is made from, formulated from, or chosen from the recited composition. *Id.* The Examiner also rejects claim 1 for unacceptable Markush language. *Id.* Claim 2 is rejected for lack of clarity with respect to whether the patient is the same as in claim 1 from which claim 2 depends. Office action page 5. Claim 4 is rejected because the Examiner considers the language awkward. *Id.* Claim 8 is rejected for lack of antecedent basis for the limitation "the concentration". *Id.*

Although Applicants believe the claims as originally presented particularly pointed out and distinctly claimed Applicant's invention, in the interest of expediting prosecution Applicants have amended the claims to address the Examiner's concerns. In particular, Applicants note with respect to the amendment of claim 1 that M.P.E.P. § 2173.05(h)(II) indicates that it is acceptable to recite "collagen or decorin" without the use of Markush language. The amendment to claim 4 is supported on page 14 at the first full paragraph, which discloses that the stabilizing agent controls fibril diameter. Claim 8 as amended clarifies that antecedent basis exists in claim 1 by further defining the stabilizing agent of claim 1. Applicants therefore respectfully request that the Examiner withdraw the rejection under 35 U.S.C. § 112, second paragraph, as applied to the amended claims.

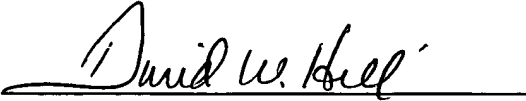
CONCLUSION

In view of the foregoing amendments and remarks, Applicants respectfully request reconsideration and reexamination of this application and the timely allowance of the pending claims. Please grant any extensions of time required to enter this response and charge any additional required fees to our deposit account 06-0916.

Respectfully submitted,

FINNEGAN, HENDERSON, FARABOW,
GARRETT & DUNNER, L.L.P.

Dated: September 27, 2004

By: 

David W. Hill
Reg. No. 28,220
(571) 203-2753

Attachments: New Abstract

ABSTRACT

Two types of compositions having an eye-drop delivery system are used during or after an orthokeratology procedure to prevent or retard relaxation of corneal tissue back to the original anterior curvature of the cornea. Each composition functions independently from the others and is a different approach of preparing a stabilizing agent. The first composition is directed to a biologically compatible composition comprising fibril associated collagens with interrupted triple helices (FACITs) and/or small leucine-rich repeat proteoglycans (SLRPs). The fibril associated collagen family includes various types of collagens, such as type VI, type XX, type XII, and type XIV. The small leucine-rich repeat proteoglycans family includes decorin, keratocan, biglycan, epiphykan, lumican, mimecan, and fibromodulin. The second composition includes the enzyme found as a normal component of tissues, plasma, or epidermis, such as transglutaminase.



The Internalization of Posterior Subcapsular Cataracts (PSCs) in Royal College of Surgeons (RCS) Rats. I. Morphological Characterization

Kristin J. Al-Ghoul,¹Kurt L. Peterson,¹Jer. R. Kuszak^{1,2}

Departments of ¹Pathology and ²Ophthalmology, Rush-Presbyterian-St. Luke's Medical Center, Chicago, IL

Purpose: To document lens ultrastructure during and after internalization of posterior subcapsular cataracts (PSCs) in Royal College of Surgeons (RCS) rats, a model for human autosomal retinal degenerative disease.

Methods: RCS rat lenses at 2, 2.5, 3, 4, 6, 9, 12, and 15 months old were enucleated and fixed. For light and transmission electron microscopy (TEM), lenses were embedded in epoxy and sectioned along the visual axis. For scanning electron microscopy, lenses were dissected to expose the posterior fibers in concentric growth shells down to the internalized PSC plaques.

Results: Overgrowth of the plaque began between 8 and 9 weeks postnatal and proceeded from the periphery to the posterior pole. This is in contrast to PSC formation which begins centrally and enlarges radially between 4-6 weeks postnatal. Peripheral-to-central overgrowth resulted in the formation of a convexo-concave, disk-shaped suture plane oriented parallel to the capsule. The initial fibers overlying the plaque were extremely flattened at their posterior ends. However, by 3 months postnatal, fiber ultrastructure was relatively normal and displayed only minor morphological irregularities. These temporal and structural changes were used to create 3-dimensional computer assisted-drawing (3D-CAD) reconstructions and animations. TEM examination of plaques revealed scattered fiber defects such as membrane whorls, globular aggregates and intracellular voids in both the internalized plaques and the initial overgrowth. The internalized PSC plaques had comparable morphology in all animals, regardless of age. Specifically, the posterior segments of fibers were enlarged and curved abnormally toward the capsule.

Conclusions: PSC plaques are not internalized and broken down in the classical cell biological sense (i. e. via lysosomal degradation). Rather the plaques retain their structure indefinitely as lens growth proceeds (albeit not entirely normally). This demonstrates that the lens has a restricted ability to respond to growth defects and effect a limited recovery after PSC formation.

The Royal College Of Surgeons (RCS) rat is an animal model for autosomal recessive retinitis pigmentosa (ARRP) wherein the retinas of RCS rats spontaneously degenerate between 2 and 6 weeks postnatal [1,2]. These animals also develop bilateral posterior subcapsular cataracts (PSCs) which can be detected by slit lamp examination at 7-8 weeks of age [3]. Hence, the RCS rat is also a useful model for PSC associated with ARRP.

Our recent investigation of RCS rat PSCs [4] demonstrated that cataract formation occurs from four to six weeks postnatal and results from a growth malformation affecting the posterior segments of elongating fibers. Specifically, the posterior fiber ends curve away from the polar axis toward the vitreous and enlarge into ovate globules under the capsule, forming a PSC plaque. Consequently, plaque formation precludes normal posterior suture formation during posterior subcapsular cataractogenesis.

It has been reported that subsequent to PSC formation, 75% of animals "recover" by internalizing the PSC plaque via new growth, while the remaining 25% of animals develop mature cataracts by 9-12 months of age [3]. In lenses with internalized PSCs, new fiber growth over the PSC plaque is

transparent and thus has been characterized as healthy [5]. However, transparency alone does not ensure good optical quality. Recent structural analyses in various types of lenses has shown that excessive disorder due to abnormal suture formation is correlated with a decrease in optical quality [6-8]. The aim of this investigation was to characterize the ultrastructure of internalized PSCs and the posterior portions of overlying lens fibers as a function of time after internalization.

METHODS

Lenses: RCS rat lenses at 2, 2.5, 3, 4, 6, 9, 12, and 15 months (n = 6-8 animals per group) were utilized in this investigation. All animals were treated in accordance with the ARVO Statement for the Use of Animals in Ophthalmic and Vision Research. Animals were euthanized by intra peritoneal injection of sodium pentobarbital and the eyes were enucleated. The tissue posterior to the ora serrata was removed and the remaining anterior portion of the eye was immediately placed into fixative. Some RCS rat lenses were obtained from breeding colonies maintained at Alcon Laboratories Inc., Ft. Worth, Texas and at Columbia University, NY (kindly provided by Dr. K. Bhuyan). In these cases, lenses were placed in fixative after enucleation and dissection from the orbit, then shipped to the laboratory by overnight express.

Fixation: Lenses were fixed by one of two methods: (1) 24 hours in 10% buffered formalin, then 2 days in 2.5% glut-

Correspondence to: K. J. Al-Ghoul, Ph.D., Department of Pathology, Rush-Presbyterian-St. Luke's Medical Center, 1653 West Congress Parkway, Chicago, IL, 60612; Phone: (312) 942-6871; FAX: (312) 942-2371; email: kalghoul@rush.edu

araldehyde in 0.07 M sodium cacodylate buffer with fresh fixative daily, or (2) 3 days in 2.5% glutaraldehyde in 0.07 M sodium cacodylate buffer with fresh fixative daily. All lenses were washed overnight in 0.2 M sodium cacodylate buffer, then examined under a dissecting microscope (Zeiss, New York, NY) and photographed. Color slides of whole lenses were digitized using a Polaroid Sprint Scan 35 (Polaroid Corp., Bedford, MA) operated with Adobe Photoshop version 5 (Adobe Systems Inc., San Jose, CA) on a pentium pc platform.

Scanning Electron Microscopy: To expose the PSCs, lenses were either split along the optic axis or dissected as previously described [4]. Briefly, superficial fibers were peeled away from the lens around its entire diameter, resulting in crescent-shaped groups of fibers and the remaining lens core. Subsequent layers of fibers were removed in the same manner until the internalized PSC was visible on the lens core. Both the superficial fiber "peels" and the remaining lens mass were collected and processed for SEM.

Specimens were post-fixed in 1% aqueous osmium tetroxide at 4 °C overnight, washed in cacodylate buffer, and dehydrated through a graded ethanol series. After overnight dehydration in absolute ethanol, the alcohol was replaced through a graded series of Freon 113. Specimens were critical point dried in Freon 13 in a Balzers CPD 020 (Balzers, Hudson, NH), secured on aluminum stubs with silver paste, sputter coated with gold and examined in a JEOL JSM 35c scanning electron microscope (JEOL USA, Peabody, MA) at 15 kV.

Light Microscopy/Transmission Electron Microscopy: Lenses were post-fixed overnight in 1% aqueous osmium tetroxide at 4 °C, then washed in cacodylate buffer and dehydrated through a graded ethanol series to propylene oxide. Lenses were infiltrated and flat-embedded in epoxy resin. For light microscopy, embedded lenses were bisected along the optic axis with a jeweler's saw and 1-2 μ m thick sections were cut using a glass knife. Sections were stained with a 1:1 mixture of methylene blue and azure II, then mounted on glass slides with permount. Light micrographs were taken on an

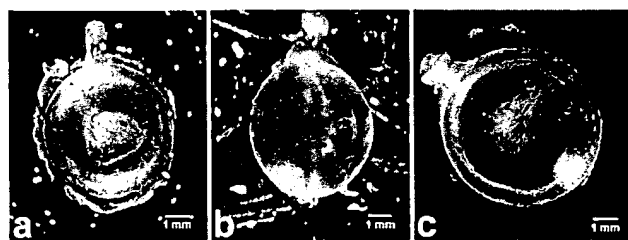


Figure 1. Light micrographs of whole, fixed RCS rat lenses. (A) The posterior aspect of a 3 month old lens showing a PSC plaque. Because internalization of the PSC commences between 8 to 10 weeks, the plaque is only covered by about 0.2 mm of new growth and consequently still appears very prominent. (B) An equatorial view of a 6 month old lens demonstrating the internalized plaque (arrow) covered by approximately 0.5 mm of new growth. (C) Posterior view of a six month old lens showing an abnormal suture pattern. Instead of the typical inverted Y pattern, this lens had a smaller, 5-branched suture pattern.

Olympus Vanox AHBS3 photographic microscope (Olympus America Inc., Melville, NY).

For TEM, mesas were positioned to include portions of both the PSC plaque and the initial overgrowth. Thin sections were cut at 60 nm with a diamond knife (Diatome, Ft. Washington, PA) on a Sorvall Ultratome V 2088 microtome (LKB, Washington, DC). Sections were mounted on uncoated 200 mesh Hex grids (Electron Microscopy Sciences, Ft. Washington, PA), stained with uranyl acetate and lead citrate, then examined on a JEOL JEM-1200EX transmission electron microscope (JEOL USA, Peabody, MA) at 60 kV.

RESULTS

Whole lenses from 2 to 3 month old RCS rats displayed superficially located speckled posterior opacities (Figure 1A). When viewed along the equatorial axis (Figure 1B), the PSCs were located progressively deeper within the lens as a function of time. Although fibers overgrowing the PSC were trans-

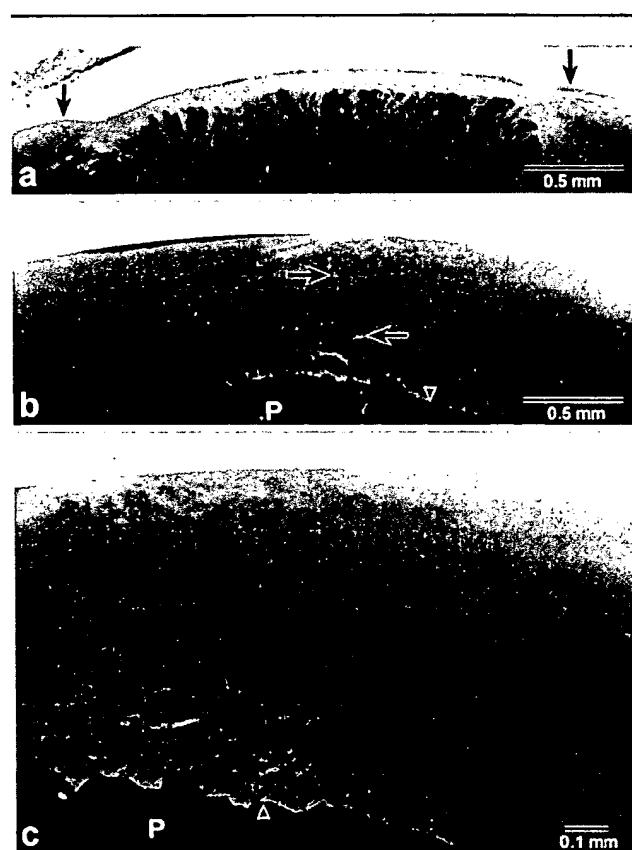


Figure 2. Light micrographs of thick axial sections at the posterior pole during the initial stages of PSC internalization. (A) At 2 months postnatal, new fiber growth had accumulated at the periphery of the plaque (arrows) but had not yet overgrown the PSC. (B,C) Non-adjacent serial sections from a 3 month old RCS rat lens. The plaque (P) was completely internalized by new fiber growth. The suture plane formed subsequent to plaque overgrowth is demarcated by arrows (B). At higher magnification (C) it can be seen that overgrowth of the plaque began marginally and advanced to confluence at the pole. The posterior ends of new fibers interfaced with the upturned ends of fibers in the plaque, forming a convexo-concave, disk-shaped suture plane parallel to the capsule (arrowheads).

parent, posterior suture formation was abnormal as indicated by the lack of a typical inverted Y pattern (Figure 1C).

Light microscopy of thick axial sections demonstrated that at 2 months postnatal, new fiber growth had accumulated adjacent to the plaque (Figure 2A, arrows). The posterior ends

of upturned fibers comprising the PSC plaque were separated from the capsule. At 3 months postnatal, the plaque was com-

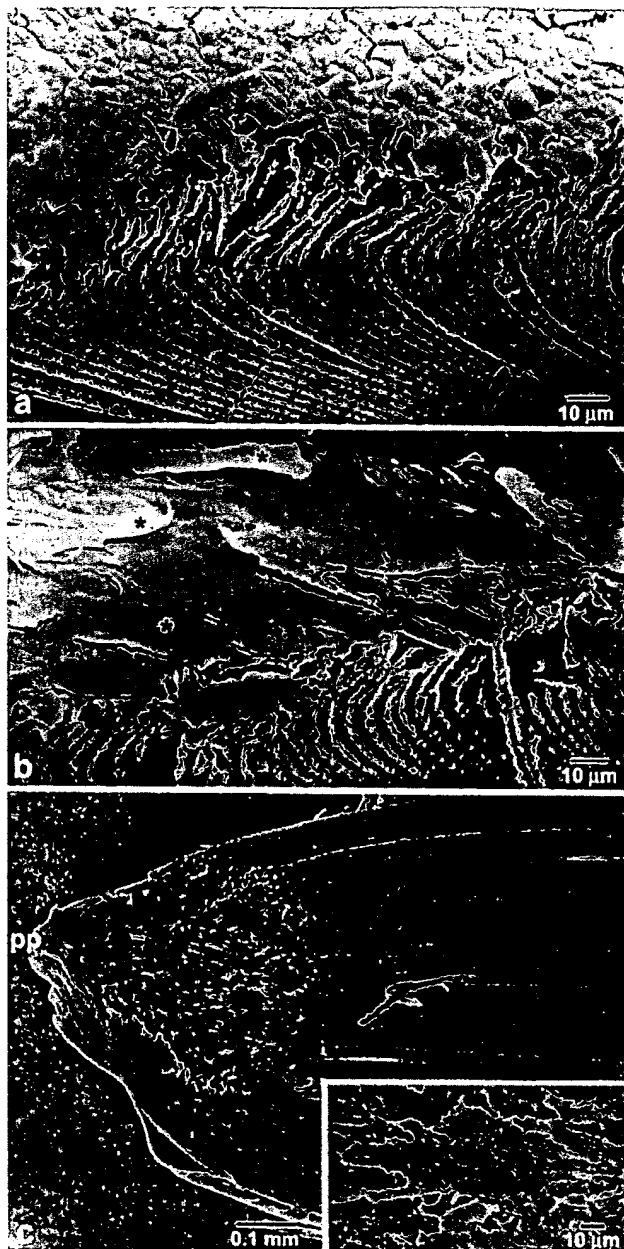


Figure 3. Scanning electron micrographs depicting the morphology of the initial fibers overlying the plaque in 2.5-3 month old lenses. (A,B) The posterior ends of fibers overlying the plaque were extremely flattened (asterisks). (C) The posterior portion of a fiber peel obtained from dissection of a 3 month old RCS rat lens. Even at low magnification it was apparent that fiber morphology was normal along fiber length but not over the plaque. During internalization of the PSC, each successive shell of fibers terminated progressively closer to the posterior pole (PP), resulting in peripheral to central overgrowth of the plaque. Higher magnification (inset) demonstrating the irregular, branched, terminal extensions of fiber ends overlying the plaque.

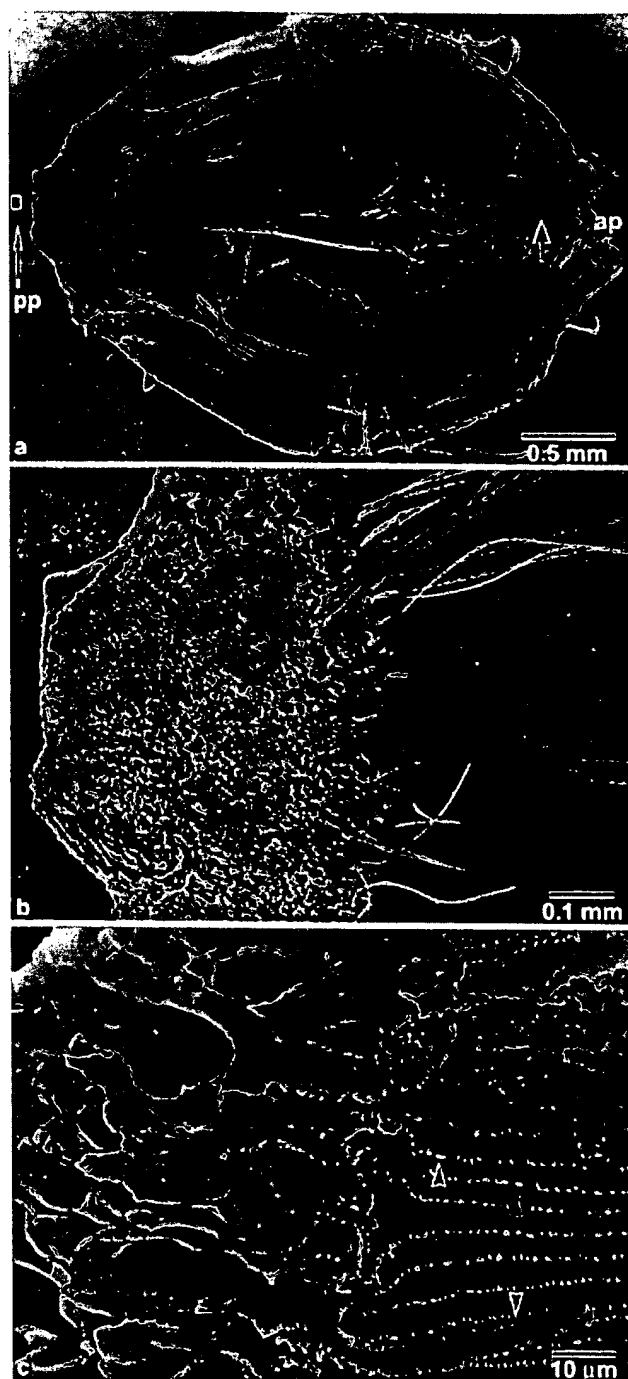


Figure 4. Scanning electron micrographic magnification series of a fiber peel taken from a 2.5-month old RCS rat lens. A view of the entire peel (A) shows fibers that had approached the anterior pole (AP) displayed normal opposite end curvature to form a suture branch (arrow), whereas fibers that had approached the posterior pole (PP) interfaced with the ends of upturned fibers in the plaque. Note that the overgrowth had not yet reached the posterior pole in this specimen. At higher magnification (B), the posterior ends of fibers directly over the plaque displayed concavities which were complementary to the enlarged ends of fibers comprising the plaque. The posterior ends of fibers also lacked fiber-fiber interdigitations (C) which were present along the rest of the fiber length (arrowheads).

pletely internalized by growth of new fibers (Figure 2B). Overgrowth of the PSC began at the perimeter of the plaque and progressed centrally to confluence at the posterior pole. During overgrowth of the plaque, the posterior ends of new fibers abutted with the enlarged fiber ends in the plaque (Figure 2C), forming an abnormal, convexo-concave, disk-shaped suture plane oriented parallel to the capsule (with the convex surface facing the posterior). After the PSC plaque was completely overgrown, new fibers abutted with each other in the conventional manner [9,10] to form suture planes perpendicular to the capsule (Figure 2B, arrows). However, as demonstrated in Figure 1C, posterior suture patterns were not normal. The functional implications of abnormal suture formation during PSC internalization have been explored in a concurrent investigation [11].

Scanning electron microscopic examination of the initial fibers overlying the plaque showed that their posterior ends were extremely flattened (Figure 3A,B, asterisks) and had irregular, branched, terminal extensions (Figure 3C, inset). This is in contrast to the slightly-flared fiber ends characteristically seen at sutures [12]. Inspection of fiber peels obtained during lens dissections revealed that fiber morphology was normal except over the plaque (Figure 3C and Figure 4A-C). In some lenses, the posterior ends of fibers directly over the plaque displayed concavities which were complementary to the enlarged ends of fibers comprising the plaque. The concave ends of fibers also lacked fiber-fiber interdigitations (Figure 4C, arrowheads) which are typically present both at fiber ends and along the rest of the fiber length in rat lenses [4,12]. In addition, it was apparent that during internalization of PSCs, each successive growth shell of fibers terminated closer to the posterior pole (Figure 3C and Figure 4A,B).

Transmission electron microscopic observations of the plaque and initial overgrowth were completely consistent with



Figure 5. Transmission electron micrograph of the internalized PSC at 3 months postnatal. A low magnification overview demonstrates the enlarged, ovate ends of fibers in the plaque (asterisks), the thin, irregular fibers that covered the plaque (squares) and the flattened hexagonal profiles of relatively normal fibers from more external growth shells (black dots).

features noted by light and scanning electron microscopy. The ovate profiles of fiber ends in the plaque were overlain by attenuated, irregularly-shaped fiber ends which, in turn, were overlain by flattened, hexagonal profiles typical of cross-sectioned fibers (Figure 5). Scattered defects such as membrane whorls, intracellular voids, and small globules were located in both the plaque and initial overgrowth (Figure 6). However, there was no evidence of wide-spread breakdown of the internalized PSC.

Precise dissection of RCS rat lenses to a diameter of 2.5 mm (equivalent to 6 weeks postnatal) exposed the internalized plaques for SEM evaluation. In animals 3 to 15 months old, internalized plaques were structurally similar regardless of the length of time since internalization occurred (Figure 7). Specifically, the plaques were composed of enlarged, globulized fiber ends abnormally curved towards the capsule at all ages examined.

DISCUSSION

In this study, correlative LM, SEM and TEM have elucidated the structure of RCS rat lenses during and after PSC internal-

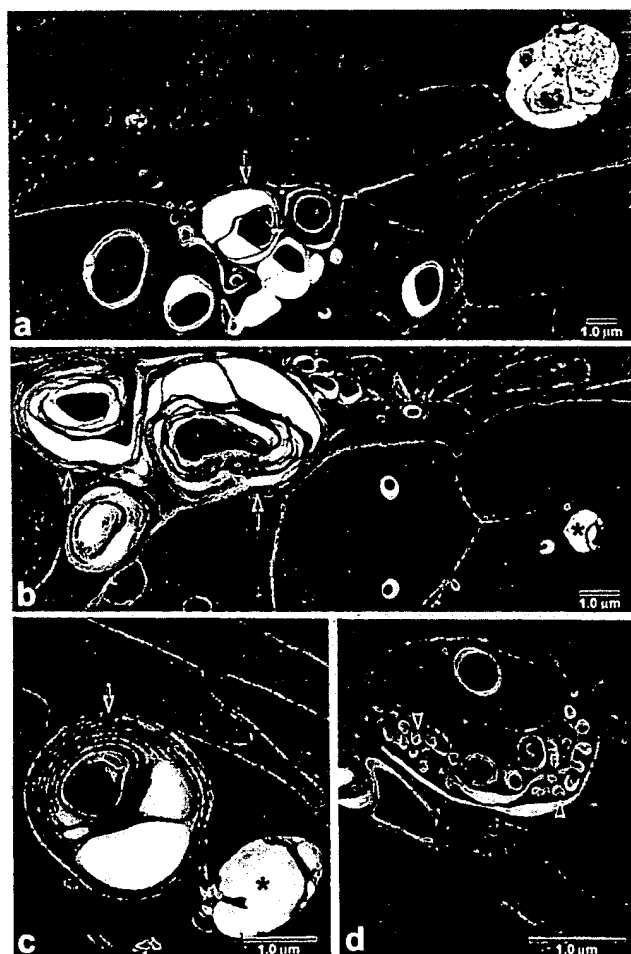


Figure 6. Transmission electron micrographs of morphological defects in the internalized plaque and early overgrowth in RCS rat lenses. (A-D) Commonly observed defects included membrane whorls (arrows), intracellular voids (asterisks) and small globules (arrowheads).

ization. Precise characterization of fiber morphology throughout PSC formation [4] and internalization was utilized to create 3-D CAD reconstructions (Figure 8 and Figure 9) and an animation (Figure 10) depicting these events. Figure 8 summarizes PSC formation from 2 to 6 weeks. Figure 9 outlines the initial internalization of PSC plaques from 8 to 12 weeks. The 3D-CADs in Figure 8 demonstrate that the PSC was due to a growth malformation which affects the posterior segments of each successive growth shell of fibers, resulting in gradual plaque formation. In a similar manner, as shown in Figure 9, plaque internalization was accomplished progressively as each new growth shell of fibers extends closer to the posterior pole. The rate of PSC formation and internalization was therefore dependent on the growth rate of the affected lens (and would be expected to be more rapid in juvenile rat lenses as compared to mature human lenses).

The initial internalization of the PSC created an abnormal suture plane parallel to the capsule and essentially perpendicular to the optic axis. Since sutures are regions of naturally occurring disorder which have a measurable negative effect on lens optics [6-8], the addition of an abnormal suture plane directly across the optic axis would be expected to adversely affect lens function. In fact, laser scan analysis of

recovered RCS rat lenses implied that the light path was obscured in central locations [11]. Conversely, there are two factors which may exert a positive influence on the optics of recovering lenses. First, the posterior ends of new fibers formed concavities which covered the irregular surface of the plaque, effectively minimizing extracellular space between the two disparate regions. Second, relatively normal fiber morphology was reestablished rapidly (within only a few growth shells), restoring the ordered array of radial cell columns and suture patterns which are optimal for lens optics. Once again, analysis of the optical quality of RCS rat lenses after recovery from PSC confirms the importance of correctly-formed suture patterns in minimizing light diffraction [11].

It is generally presumed that human PSCs, regardless of etiology, are the result of dysplastic cells which migrate posteriorly and aggregate at the posterior pole. However, recent evidence indicates that this may be incorrect for PSC associ-

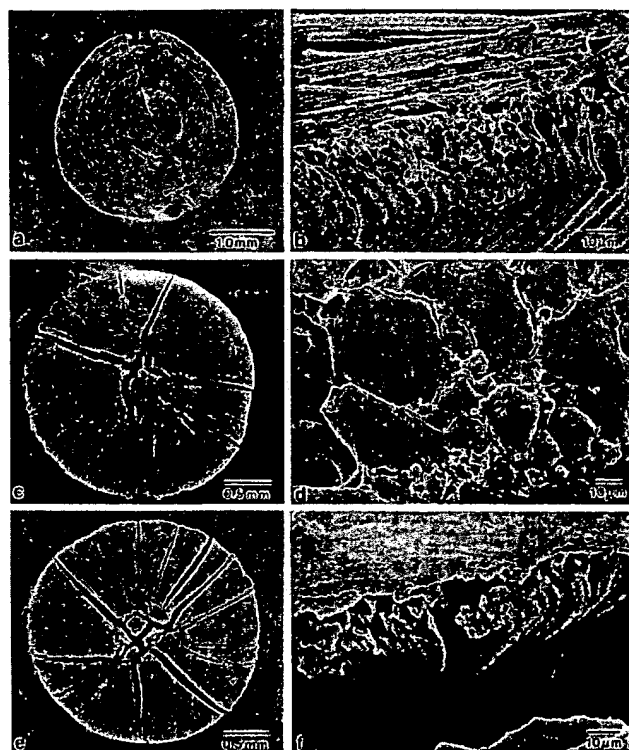


Figure 7. Scanning electron micrographs of internalized plaques at 4, 9, and 15 months old. The PSC plaques displayed consistent structural features at all ages examined. Specifically, the plaques were composed of markedly enlarged and irregular posterior fiber ends aberrantly curved toward the capsule. (A) 4 month old lens split along the optic axis. (B) Enlargement of boxed area in (A). (C) 9 month old lens dissected to expose the PSC. (D) Enlargement of boxed area in (C). (E) 15 month old lens with the PSC partially exposed. (F) Enlargement of boxed area in (E).

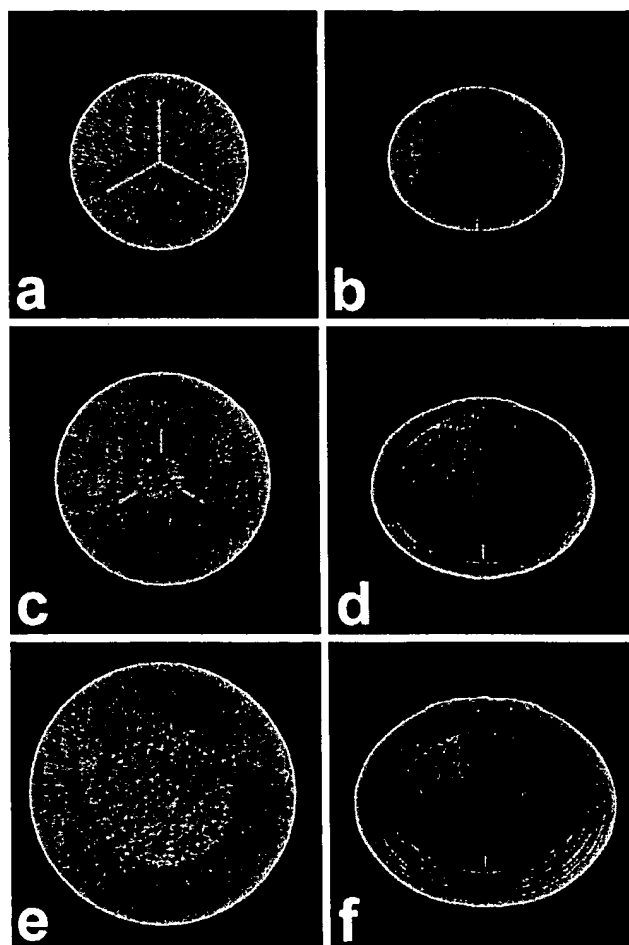


Figure 8. Scale 3D-CAD reconstructions of PSC development in RCS rats. Posterior subcapsular cataractogenesis occurs between 2 and 6 weeks postnatal. At 4 weeks, most lenses had a small, polar opacity which enlarged radially to a large PSC plaque by 6 weeks. The plaque was formed by posterior fiber ends which curved abnormally toward the vitreous and globulized under the capsule. PSC formation precluded development of normal posterior sutures. A posterior view is shown in (A,C,E). An axial view is shown in (B,D,F).

(A,B) 2 weeks postnatal. (C,D) 4 weeks postnatal. (E,F) 6 weeks postnatal.

ated with retinal degenerative disease and for post-vitrectomy PSC. In both the present model (RCS rat) and in a transgenic mouse model for autosomal dominant retinitis pigmentosa, there was no evidence of posterior migration of nucleated cells [4,13]. Rather, the PSCs were formed by abnormal posterior fiber growth. Similarly, in a rabbit model for post-vitrectomy PSC, cataracts were due to abnormal posterior suture development rather than posterior migration of cells from the bow region (unpublished data, Kuszak et al.). In addition, it has long been recognized that some PSCs noted clinically have a stellate appearance, indicating involvement of the sutures in posterior opacification [14,15]. This suggests that there may be two types of PSC: one caused by posterior migration of

dysplastic cells, and one caused by abnormal fiber growth resulting in posterior sutural malformations.

SEM examination of 3 to 15 month old lenses indicated that the structure of internalized plaques remained stable throughout the life span of animals. Similarly, TEM examination of internalized plaques revealed only scattered ultrastructural defects. It is clear that the fibers comprising PSC plaques were neither internalized nor broken down via lysosomal degradation, as occurs during internalization of necrotic and senescent cells in other tissues [16-18]. The sparse ultrastructural damage located within the plaque and initial overgrowth in RCS rats is dissimilar to previous observations of human PSC associated with retinal degenerative disease [19-21] which described widespread fiber degeneration in the posterior region. Human lens observations in those studies are more consistent with observations from RCS rat lenses which do not recover, but instead progress to mature cataracts [22].

The results of this investigation demonstrate that the lens has the ability, although restricted, to respond to growth defects and effect a limited recovery after PSC formation associated with retinal degeneration. This is not entirely unexpected since spontaneous recovery from PSCs have been reported in diabetic patients [23-25]. Evaluation of the optical quality of internalized RCS rat PSCs has provided a quantitative measure of the extent and limitations of the recovery of lens function and is described in the concurrent investigation [11].

ACKNOWLEDGEMENTS

The authors thank Layne A. Novak for his expert technical assistance. We are also grateful to Alcon Laboratories Inc. (Ft.

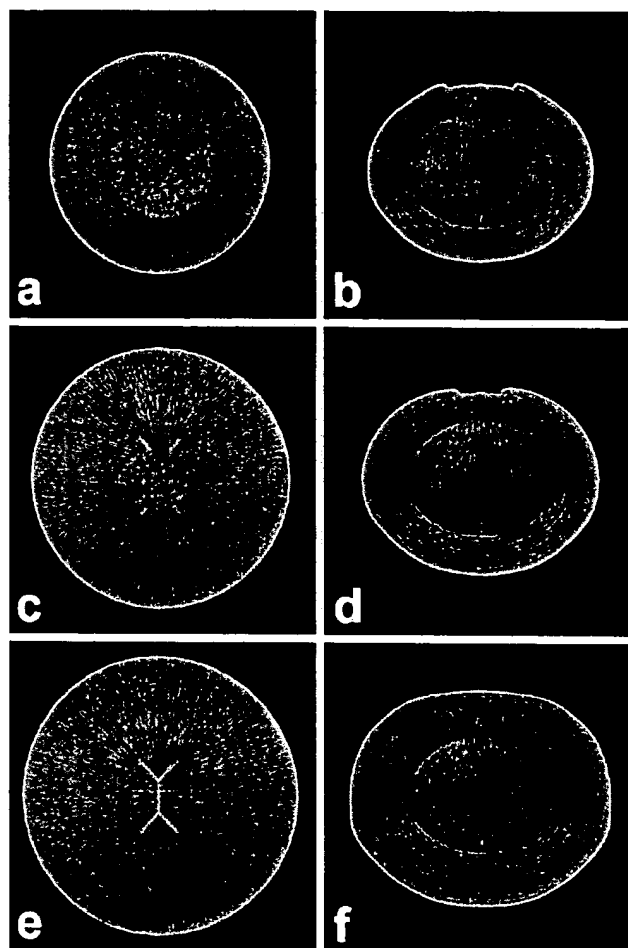


Figure 9. Scale 3D-CAD reconstructions of PSC internalization in RCS rats. Internalization of the plaque began between 2 and 2.5 months postnatal. By 2 months postnatal, new fiber growth accumulated at the perimeter of the plaque, which was separated from the capsule. The posterior ends of new fibers interfaced with fiber ends of the plaque, forming an abnormal suture plane across the visual axis. Between 2.5 and 3 months postnatal the PSC was completely covered by new fiber growth, after which fibers began forming suture planes perpendicular to the capsule. A posterior view is shown in (A,C,E). An axial view is shown in (B,D,F).

(A,B) 2 months postnatal. (C,D) 2.5 months postnatal. (E,F) 3 months postnatal.

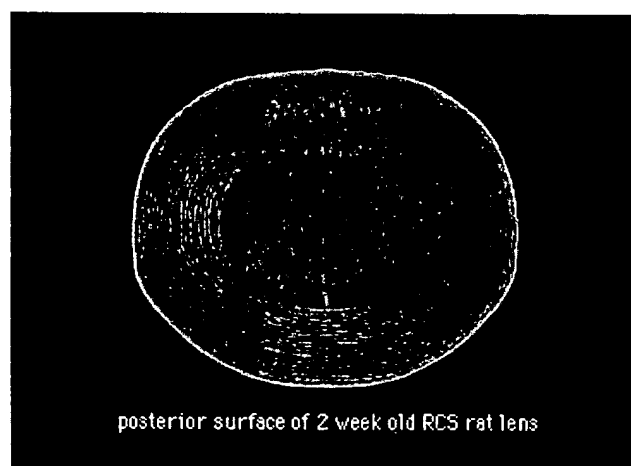


Figure 10. Scale 3D-CAD animation depicting PSC formation and initial PSC internalization in RCS rat lenses. The PSC, which develops between 2 and 6 weeks postnatal, results from a growth malformation of the posterior segments in each successive growth shell, and results in central-to-peripheral plaque formation. Similarly, the plaque is gradually internalized as each growth shell of fibers terminates closer to the posterior pole. This peripheral-to-central overgrowth occurs between 2 and 2.5 months postnatal and results in the formation of an aberrant suture plane across the visual axis.

A quicktime movie of this figure is in the online version at the following URL: <http://www.molvis.org/molvis/v5/p6/al-ghoul-figure10.html>. A representative frame is shown above.

Worth TX) and Dr. K. Bhuyan (Columbia University, NY) for providing RCS rat lenses. This work was supported by NIH-NEI grant EY-06642 to JRK and by the Louise C. Norton Trust (Chicago, IL).

REFERENCES

1. Dowling JE, Sidman RL. Inherited retinal dystrophy in the rat. *J Cell Biol* 1962; 14:73-109.
2. LaVail MM, Battelle BA. Influence of eye pigmentation and light deprivation on inherited dystrophy in the rat. *Exp Eye Res* 1975; 21:167-92.
3. Hess HH, Newsome DA, Knapka JJ, Westney GE. Slitlamp assessment of age of onset and incidence of cataracts in pink-eyed, tan-hooded retinal dystrophic rats. *Curr Eye Res* 1982-83; 2:265-9.
4. Al-Ghoul KJ, Novak LA, Kuszak JR. The structure of posterior subcapsular cataracts in the Royal College of Surgeons (RCS) rats. *Exp Eye Res* 1998; 67:163-77.
5. O'Keefe TL, Hess HH, Zigler JS Jr, Kuwabara T, Knapka JJ. Prevention of cataracts in pink-eyed RCS rats by dark rearing. *Exp Eye Res* 1990; 51:509-17.
6. Kuszak JR, Sivak JG, Weerheim JA. Lens optical quality is a direct function of lens sutural architecture [published erratum appears in *Invest Ophthalmol Vis Sci* 1992; 33:2076-7]. *Invest Ophthalmol Vis Sci* 1991; 32:2119-29.
7. Sivak JG, Herbert KL, Peterson KL, Kuszak JR. The interrelationship of lens anatomy and optical quality. I. Non-primate lenses. *Exp Eye Res* 1994; 59:505-20.
8. Kuszak JR, Peterson KL, Sivak JG, Herbert KL. The interrelationship of lens anatomy and optical quality. II. Primate lenses. *Exp Eye Res* 1994; 59:521-35.
9. Kuszak JR, Bertram BA, Macsai MS, Rae JL. Sutures of the crystalline lens: a review. *Scan Electron Microsc* 1984; (Pt 3):1369-78.
10. Kuszak JR. The development of lens sutures. *Prog Retin Eye Res* 1995; 14:567-91.
11. Kuszak JR, Al-Ghoul KJ, Novak LA, Peterson KL, Herbert K, Sivak JG. Internalization of posterior subcapsular cataracts (PSCs) in Royal College of Surgeons (RCS) rats. II. The interrelationship of optical quality and structure as a function of age. *Mol Vis* 1999; 5:7.
12. Kuszak JR, Bertram BA, Rae JL. The ordered structure of the crystalline lens. In: Hilfer SR, Sheffield JB, editors. *Development of order in the visual system*. New York: Springer-Verlag; 1986. p. 35-60.
13. Novak L, Kuszak JR, Naash MI. The structure of posterior subcapsular cataracts (PSCs) in retinal degenerative disease models. *Invest Ophthalmol Vis Sci* 1996; 37:S893.
14. Eshaghian J, Rafferty NS, Goossens W. Human cataracta complicata. Clinicopathologic correlation. *Ophthalmology* 1981; 88:155-63.
15. Eshaghian J. Human posterior subcapsular cataracts. *Trans Ophthalmol Soc U K* 1982; 102:364-8.
16. Roque RS, Imperial CJ, Caldwell RB. Microglial cells invade the outer retina as photoreceptors degenerate in Royal College of Surgeons rats. *Invest Ophthalmol Vis Sci* 1996; 37:196-203.
17. Garfield RE, Chacko S, Blose S. Phagocytosis by muscle cells. *Lab Invest* 1975; 33:418-27.
18. Marchesi VT, Furthmayr H, Tomita M. The red cell membrane. *Annu Rev Biochem* 1976; 45:667-98.
19. Dilley KJ, Bron AJ, Habgood JO. Anterior polar and posterior subcapsular cataract in a patient with retinitis pigmentosa: a light-microscopic and ultrastructural study. *Exp Eye Res* 1976; 22:155-67.
20. Eshaghian J, Rafferty NS, Goossens W. Ultrastructure of human cataract in retinitis pigmentosa. *Arch Ophthalmol* 1980; 98:2227-30.
21. Fagerholm PP, Philipson BT. Cataract in retinitis pigmentosa. An analysis of cataract surgery results and pathological lens changes. *Acta Ophthalmol (Copenh)* 1985; 63:50-8.
22. Al-Ghoul KJ, Kuszak JR. Anterior Polar Cataracts In RCS rats: a predictor of mature cataract formation. *Invest Ophthalmol Vis Sci* 1999; 40:668-79.
23. Dickey JB, Daily MJ. Transient posterior subcapsular lens opacities in diabetes mellitus. *Am J Ophthalmol* 1993; 115:234-8.
24. Phillip M, Ludwick DJ, Armour KM, Preslan MW. Transient supcapsular cataract formation in a child with diabetes. *Clin Pediatr (Phila)* 1993; 32:684-5.
25. Butler PA. Reversible cataracts in diabetes mellitus. *J Am Optom Assoc* 1994; 65:559-63.

An *in vitro* tubulogenesis system using cell lines derived from the embryonic kidney shows dependence on multiple soluble growth factors

(kidney development/ureteric bud/metanephric mesenchyme/extracellular matrix)

HIROYUKI SAKURAI*, ELVINO J. BARROS*, TATSUO TSUKAMOTO*, JONATHAN BARASCH†, AND SANJAY K. NIGAM*‡

*Renal Division, Department of Medicine, Brigham and Women's Hospital, and Harvard Medical School, Boston, MA 02115; and †Department of Medicine, College of Physicians and Surgeons, Columbia University, New York, NY 10032

Communicated by Joseph E. Murray, Wellesley Hills, MA, March 31, 1997 (received for review February 13, 1997)

ABSTRACT Interactions between the ureteric bud (UB) and metanephric mesenchyme are crucial for tubulogenesis during kidney development. Two immortalized cell lines derived from the day 11.5 embryonic kidney, UB cells, which appear to be epithelial (cytokeratin-positive, E-cadherin-positive, and ZO-1-positive by immunostaining) and BSN cells, which are largely mesenchymal (vimentin-positive, but negative for cytokeratin, cell surface E-cadherin, and cell surface ZO-1), were used to establish an *in vitro* tubulogenesis system. BSN cells expressed hepatocyte growth factor (HGF) and transforming growth factor- β 1 mRNAs, and its conditioned medium (BSN-CM) contained factors capable of activating the epidermal growth factor (EGF) receptor (EGFR). When UB cells were cultured in an extracellular matrix gel in the presence of the embryonic kidney or BSN-CM, the UB cells underwent morphogenetic changes characteristic of early *in vitro* branching tubulogenesis. These changes were largely inhibited by a combination of neutralizing anti-HGF antibodies and the EGFR inhibitor tyrphostin AG1478, suggesting that EGFR ligands, together with HGF, account for much of this early morphogenetic activity. Nevertheless, there was a significant fraction of tubulogenic activity that could not be inhibited, suggesting the existence of other soluble factors. Whereas HGF, EGF, transforming growth factor α , basic fibroblast growth factor (bFGF), and insulin-like growth factor 1 (IGF-1), or a mixture of these growth factors, induced epithelial processes for up to 3 days, only IGF-1, possibly bFGF, and the mixture were able to sustain morphogenesis for longer periods, though not nearly to the same degree as BSN-CM. Moreover, only BSN-CM induced branching tubular structures with clear lumens, consistent with the existence of other soluble factors crucial for the formation and/or maintenance of branching tubular structures with lumens *in vitro*.

In the murine embryo, metanephrogenesis is initiated when the ureteric bud (UB) interacts with undifferentiated metanephric mesenchyme around 11.5 days after conception. The UB undergoes successive dichotomous branching steps as it invades the metanephric mesenchyme, developing into the kidney collecting system and ureteric tree. The cells of the metanephric mesenchyme, which have been induced by the UB, epithelialize and ultimately develop into the more proximal nephron from the glomerular capsule to the distal tubule (1, 2). Thus, UB interactions with the metanephric mesenchyme are essential for normal kidney development. Genetic approaches have recently implicated several potentially diffusible molecules in kidney development, including wnt-4 (3) and

bone morphogenetic protein 7 (4, 5). Furthermore, organ culture studies suggest that a number of growth factors, including hepatocyte growth factor (HGF) (6), epidermal growth factor (EGF) receptor (EGFR) ligands (7), insulin-like growth factor 1 (IGF-1) (8, 9), and others, play at least a facilitatory role in kidney development. Nevertheless, the spatiotemporal complexity of cell interactions in the developing kidney makes detailed analysis of cellular processes at the level of the whole embryo or in organ culture difficult.

In vitro cell culture systems, while possessing their own particular limitations, can be used to complement genetic or organ culture approaches. To the extent that this kind of approach reflects events occurring *in vivo* during development, it can be used to gain mechanistic insights into complex morphogenetic processes. One of the best-studied models employs kidney epithelial cell lines, such as Madin–Darby canine kidney (MDCK) and murine inner medullary collecting duct (mIMCD3), seeded in three-dimensional type I collagen gels to analyze mechanisms of epithelial tubulogenesis and branching morphogenesis (10–17). In the mIMCD3 cell–collagen gel system, HGF and EGFR ligands induce branching tubulogenesis (10, 11), whereas transforming growth factor (TGF)- β selectively inhibits branching events (14). Since these cells are derived from the collecting duct (and thus ultimately the UB), the results from this system have been used to propose a model whereby gradients of growth factors which might exist within the mesenchyme or elsewhere in the developing kidney lead to vectorial branching tubulogenesis such as occurs during collecting system development (17–19). The fact that multiple growth factors are capable of inducing branching tubulogenesis has also been used to argue for “relative redundancy” and explain why knockouts of individual growth factors often fail to exhibit obvious abnormalities in kidney development (20–24). However, the mIMCD3 and MDCK cells are derived from differentiated kidney epithelial cells, and the extent to which results from these models are applicable to the embryonic kidney has not been established. A more authentic *in vitro* model would be to use epithelial cells directly from the embryonic kidney. We have therefore developed an *in vitro* tubulogenesis system using immortalized UB cells and conditioned medium from cells which appear to be derived from the embryonic kidney mesenchyme. The results obtained with this model system suggest that, in addition to HGF and EGFR ligands, which are important for branching tubulogenesis in

Abbreviations: UB, ureteric bud; HGF, hepatocyte growth factor; EGF, epidermal growth factor; EGFR, EGF receptor; IGF-1, insulin-like growth factor 1; bFGF, basic fibroblast growth factor; ECM, extracellular matrix; MDCK, Madin–Darby canine kidney; mIMCD, murine inner medullary collecting duct; TGF, transforming growth factor; GDNF, glial cell line-derived neurotrophic factor; PDGF, platelet-derived growth factor; BSN-CM, BSN cell conditioned medium.

‡To whom reprint requests should be addressed. e-mail: sknigam@bics.bwh.harvard.edu.

The publication costs of this article were defrayed in part by page charge payment. This article must therefore be hereby marked “advertisement” in accordance with 18 U.S.C. §1734 solely to indicate this fact.

© 1997 by The National Academy of Sciences 0027-8424/97/946279-6\$2.00/0

mIMCD3 cells, other known and yet-to-be-identified soluble factors play an important role in tubulogenesis *in vitro*.

MATERIALS AND METHODS

Cell Lines and Three-Dimensional Extracellular Matrix (ECM) Gel Culture. The UB cell line was obtained from microdissected UB of a day-11.5 mouse embryo transgenic for simian virus 40 (SV40) large T antigen (Immortomouse, Charles River) as described previously (25). The UB cells were maintained in MEM, supplemented with 10% fetal calf serum (FCS) at 32°C in a 5% CO₂ incubator. The BSN cell line was obtained from a day-11.5 murine embryonic kidney transgenic for the early region of SV40 [TgN(SV)7Bri, kindly supplied by R. L. Brinster, Univ. of Pennsylvania] (26). After embryonic kidneys were microdissected, the UB was carefully removed. The remaining metanephric mesenchyme was placed in DME/F12 medium, with 10% FCS at 37°C in a 5% CO₂ incubator. The cells outgrown from the metanephric mesenchyme were transferred to plastic culture dishes and subselected. These BSN cells were maintained in DME/F12 with 10% FCS at 37°C in a 5% CO₂ incubator. Passages 4–14, during which the cells appeared to have a relatively stable character by marker analysis, were used for experiments. Experiments with later passage cells had greater variability. To obtain BSN cell conditioned medium (BSN-CM), a confluent BSN cell monolayer was washed twice with serum-free DME/F12 medium, followed by application of serum-free DME/F12 and incubation in a CO₂ incubator for 2–4 days. The collected BSN-CM was centrifuged at low speed to remove cell debris. The culture conditions for mIMCD3 cells have been previously described (10, 27).

Three-dimensional culture of UB cells was performed as previously described (10, 11, 14). In some experiments UB cells were suspended in the mixture of growth factor-depleted Matrigel and type I collagen. For the embryonic kidney coculture experiment, day-13 embryonic kidneys were placed on top of ECM gels in serum-free DME/F12 medium. The morphology of the suspended UB cells was analyzed by a phase-contrast microscope with Hoffman modulator. The three-dimensional cultures were maintained in a 32° or 37°C CO₂ incubator with daily medium change for 5 days and every other day thereafter. At least morphologically, the incubation temperature did not seem to affect UB cell morphogenesis. Twenty randomly selected cells or colonies were evaluated for process formation (an early stage of tubulogenesis) or multicellular cord/tubule formation under the phase contrast microscope. The percentage of cells/colonies with processes was used as a semiquantitative indicator of tubulogenesis under each condition.

Cytochemistry for Cell Characterization. Confluent monolayers of UB and BSN cells grown on glass coverslips were prepared for immunofluorescence analysis after methanol fixation as previously described (28). Antibodies and their dilutions were as follows; mouse anti-pan cytokeratin (1:1,000, Sigma) mouse anti-vimentin (1:200, Sigma), rat anti-ZO-1 (1:1, generous gift from D. A. Goodenough, Harvard), and rat anti-E-cadherin (1:200, Sigma). In the case of staining with *Dolichos biflorus* lectin, confluent monolayers of cells grown on glass coverslips were fixed with 4% paraformaldehyde/PBS at room temperature for 15 min. After a vigorous wash with PBS (with Ca²⁺ and Mg²⁺) coverslips were incubated with Texas red-conjugated *Dolichos biflorus* lectin (50 µg/ml in Ca²⁺- and Mg²⁺-containing PBS; Sigma) at room temperature for 1 hr, followed by washing with PBS with Ca²⁺ and Mg²⁺. To determine the specificity of the lectin staining, the lectin was preincubated with *N*-acetylgalactosamine (1 mg/ml in PBS with Ca²⁺ and Mg²⁺). Coincubation with the lectin binding-sugar abolished cell surface staining. The coverslips were mounted and examined with a fluorescence microscope.

Growth Factors, Inhibitors, and Antibodies in Three-Dimensional Cell Culture. Sources and working concentrations of growth factors were as follows: HGF (R & D Systems) 40 ng/ml, EGF (Collaborative Research) 40 ng/ml, TGF-α (Collaborative Research) 40 ng/ml, basic fibroblast growth factor (bFGF; Upstate Biotechnology) 50 ng/ml, IGF-1 (Upstate Biotechnology) 50 ng/ml, glial cell line-derived neurotrophic factor (GDNF; R & D Systems) 100 ng/ml, TGF-β1 (R & D Systems) 1 ng/ml, and platelet-derived growth factor (PDGF; Upstate Biotechnology) 20 ng/ml. Growth factors were dissolved in the DME/F12 containing 0.1% BSA or 1% FCS and applied on top of the ECM gels.

The specific inhibitor for EGFR tyrosine kinase, tyrphostin AG 1478 (Calbiochem), was dissolved in dimethyl sulfoxide and applied to ECM gels at 0.3 µM. Neutralizing anti-HGF antibodies (generous gift from T. Nakamura, Osaka University, Japan) have been extensively characterized previously (6, 10). The antibodies react cleanly with HGF on Western blots, detect subnanomolar concentrations of HGF by ELISA, and inhibit HGF-induced mitogenesis (10) and tubulogenesis (6). The antibodies were applied at 10 µg/ml.

Western Blot Analysis. Subconfluent mIMCD3 cells were stimulated with BSN-CM or EGF (20 ng/ml) for 5 min in the presence or absence of tyrphostin AG 1478 (0.3 µM). Tyrphostin AG 1478 was added 10 min before applying growth factors. Subsequently cells were lysed and subjected to SDS/PAGE as described previously (14, 28, 29). The membrane was probed with anti-phosphotyrosine antibodies (4G10, Upstate Biotechnology), followed by immunodetection.

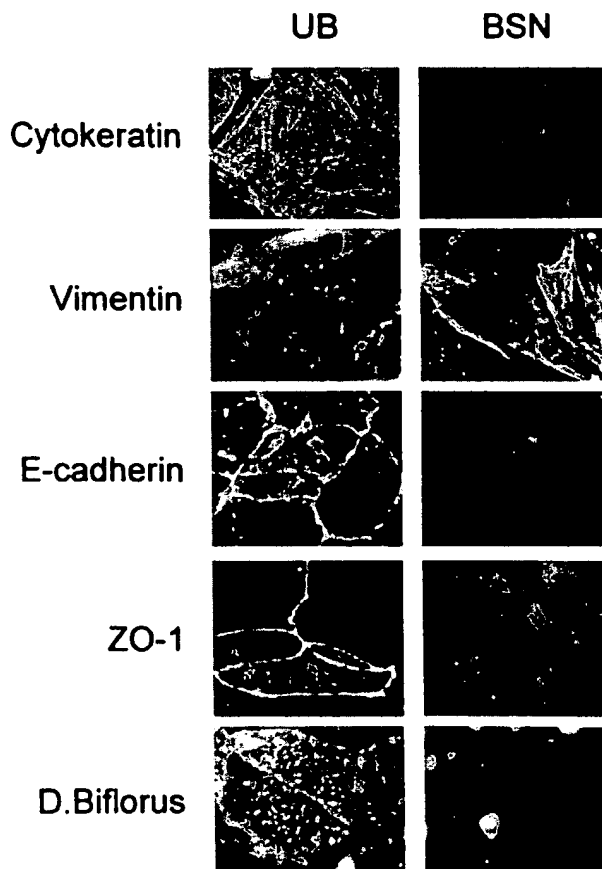


FIG. 1. Immunocytochemical characterization of UB and BSN cells. Confluent monolayers of UB and BSN cells were stained for cytokeratin, vimentin, E-cadherin, ZO-1, and binding of *Dolichos biflorus* lectin. (×450.)

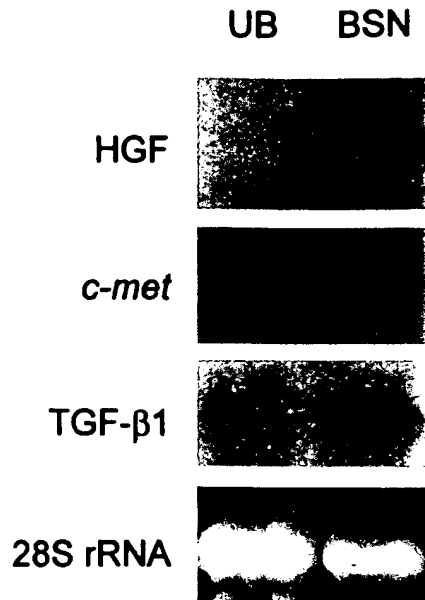


FIG. 2. Northern blots of total RNA extracted from UB and BSN cell monolayers were probed for HGF, *c-met*, and TGF- β 1. Ethidium bromide staining of 28S rRNA was used to estimate RNA loaded in each lane.

Northern Blot Analysis. Total RNA was extracted from confluent monolayers of UB and BSN cells by the acid/guanidine/phenol/chloroform method (30), followed by 1% agarose/formaldehyde gel electrophoresis. After transfer to a nylon membrane, the blot was hybridized with a 32 P-labeled cDNA probe. Probes were as follows: HGF (generous gift from M. Park, McGill University), *c-met* (generous gift from M. Park), and TGF- β 1 (generous gift from K. Totsune, Brigham and Women's Hospital).

RESULTS

Characterization of UB and BSN Cell Lines. The BSN cell line was established as described above. To determine whether it was of epithelial or mesenchymal character, both it and the UB cell line were analyzed for the expression of E-cadherin, ZO-1, cytokeratin, and vimentin as well as lectin binding. As shown in Fig. 1, UB cells were cytokeratin-positive, E-cadherin-positive, ZO-1-positive, and partially (5–30%, depending on passage) vimentin-positive, consistent with an epithelial character as previously described (25). In contrast,

BSN cells (passage 4–14) were negative for cytokeratin, though strongly positive for vimentin, consistent with a mesenchymal character. No cell surface staining for E-cadherin or ZO-1 was observed, though some faint cytoplasmic staining of ZO-1, which has been reported for a number of mesenchymal cell lines (31), was observed. The UB cells were also positive for cell surface staining by *Dolichos biflorus* lectin, known to bind a cell surface glycoprotein expressed in developing ureter but not mesenchyme, whereas BSN cells were negative for lectin staining (Fig. 1). The stain appeared to be specific, since preincubation with *N*-acetylgalactosamine eliminated the signal. We also examined HGF/*c-met* expression in these cells by Northern blotting. The UB cells were HGF-negative, *c-met*-positive, whereas the BSN cells were both HGF- and *c-met*-positive (Fig. 2). The BSN cells also expressed TGF- β 1 mRNA. Together, these results confirm the origin and epithelial character of the UB cells derived from day-11.5 UB and the largely nonepithelial character of the BSN cells derived from embryonic kidney mesenchyme of approximately the same gestational day. In addition to expressing an intermediate filament and junctional molecule profile consistent with mesenchymal origin, the BSN cells also express mRNAs for growth factors believed to be made in the embryonic kidney mesenchyme (32, 33).

BSN-CM Induced UB Cell Tubulogenesis Comparable to That Induced by the Embryonic Kidney. MDCK and mIMCD3 cells are known to undergo impressive branching morphogenesis when cocultured in ECM gels with the embryonic kidney (in the absence of apparent cell–cell contact between the embryonic kidney and the MDCK or mIMCD3 cells) due to the elaboration of soluble growth factors, including HGF and EGFR ligands (6, 10). When day-13 embryonic kidneys were placed on top of ECM gels containing UB cells, the embryonic kidneys were able to induce UB cell processes and multicellular cords, early steps in tubulogenesis *in vitro*. Thus, the embryonic kidney elaborates soluble factors capable of inducing UB cell morphogenesis; presumably these factors are in large part made in the mesenchyme. To determine if the BSN cells, which appear to be of mesenchymal origin, elaborated similar factors, BSN-CM was added to UB cells in three-dimensional ECM gel culture. A morphogenetic response comparable to that induced by the embryonic kidney was observed. The best response was obtained when the ECM gel consisted of 80% type I collagen mixed with 20% growth factor-reduced Matrigel (Fig. 3A and B). However, pure growth factor-reduced Matrigel suppressed tubule formation; instead, the matrix material promoted cyst formation even in the presence of BSN-CM (Fig. 3C). Similar modulation of tubulogenesis by ECM has been reported on MDCK cells in the presence of HGF (16). To determine whether the growth



FIG. 3. UB cells exhibit multicellular cords, tubules with lumens, and multicellular cysts in ECM gels in BSN-CM, depending on matrix composition. UB cells were suspended in 80% collagen type I/20% growth factor reduced Matrigel in the presence of BSN-CM containing 1% FCS. (A) After 7 days of culture, the cells grew to form multicellular cord-like structures. (B) After 15 days of culture, clear lumens could be seen in UB tubules. (C) When UB cells were suspended in 100% growth factor reduced Matrigel, even in the presence of BSN-CM and 1% FCS, they remained multicellular cysts even after 15 days of culture. (Bar = 50 μ m.)

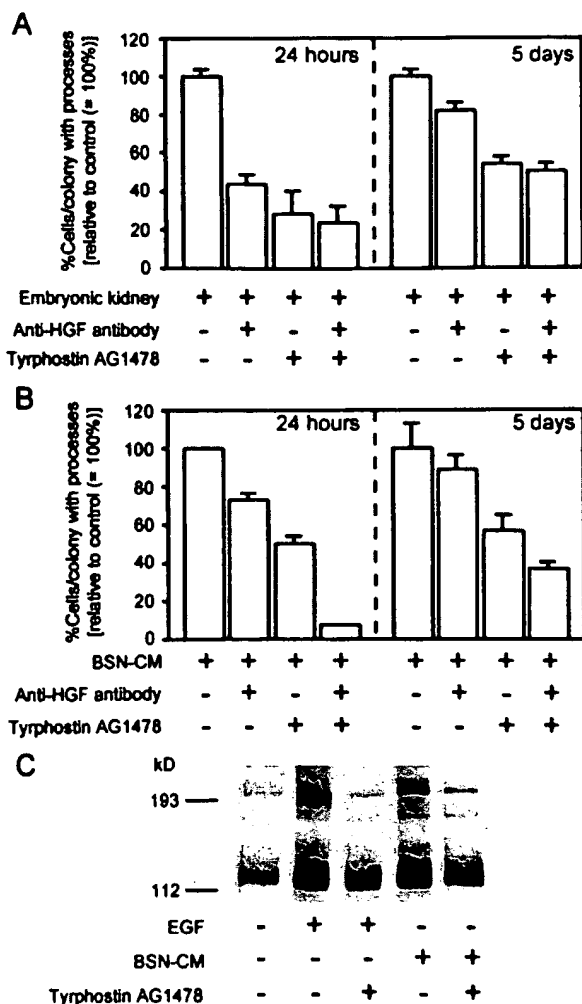


FIG. 4. BSN-CM shows tubulogenic activity comparable to that elaborated by the embryonic kidney upon UB cells grown in three-dimensional ECM gels. The percentages of UB cells/colonies exhibiting processes (an early step in tubulogenesis) were used for semi-quantitative measures of tubulogenic activity under each condition. The percentages were standardized to untreated control (= 100%) and presented as means \pm SE. The results were representative of four separate experiments. (A) Day-13 embryonic kidneys were placed on top of the three-dimensional collagen gel culture system. UB cell tubulogenesis was evaluated at 24 hr and 5 days of culture. At 24 hr, a large portion of tubulogenic activity was inhibited by a combination of neutralizing anti-HGF antibodies (10 μ g/ml) and the EGFR inhibitor tyrphostin AG 1478 (0.3 μ M). However, at 5 days about 50% of tubulogenic activity could not be inhibited. (B) BSN-CM with 1% FCS was applied on top of UB cells in three-dimensional collagen gel culture. As was the case for embryonic kidney coculture, there were differences between 24 hr and 5 days in terms of tubulogenic inhibition profile by anti-HGF antibodies and tyrphostin AG 1478. (C) BSN-CM phosphorylated tyrosine residues of EGFR. A subconfluent mIMCD3 cell monolayer was stimulated with EGF (20 ng/ml) or BSN-CM in the presence or absence of tyrphostin AG 1478 (0.3 μ M). The whole cell lysates were subjected to Western blotting with anti-phosphotyrosine antibodies. In the second (EGF) and fourth (BSN-CM) lanes, \sim 190-kDa protein was phosphorylated. The phosphorylation was completely inhibited by tyrphostin AG 1478 (third and fifth lanes).

factors promoting UB cell morphogenesis that had been secreted by the embryonic kidney and/or BSN cells were the same as those which induce mIMCD3 cell tubulogenesis, we attempted to neutralize the activity of HGF and EGFR ligands separately and together with a well-characterized anti-HGF antibody that is known to inhibit the mitogenic and tubulo-

genic activity of HGF (6, 10) and a specific EGFR tyrosine kinase inhibitor, tyrphostin AG 1478, thus far not reported to inhibit the activity of any other tyrosine kinase (34, 35). Western blots with anti-phosphotyrosine antibodies confirmed the ability of tyrphostin AG 1478 to virtually completely inhibit EGFR autophosphorylation (Fig. 4C). At 24 hr, incubation with the neutralizing anti-HGF antibodies had an inhibitory effect on the ability of the embryonic kidney or the BSN-CM to induce process formation, the earliest step in *in vitro* tubulogenesis. Tyrphostin AG 1478 had a similar inhibitory effect. Both agents together were able to inhibit all but a small fraction of the soluble morphogenetic activity elaborated by the embryonic kidney and BSN cells, suggesting that HGF and EGFR ligands together account for the largest proportion of activity involved in early process formation in this system (Fig. 4A and B left panels). To examine the effect of prolonged inhibition of HGF and EGFR, coculture was continued for up to 5 days. Anti-HGF antibodies were replaced every day. Although we administered tyrphostin AG 1478 only at the beginning of culture, its continuous presence prevented TGF- α -induced morphogenesis, suggesting long-term EGFR inactivation (data not shown). Continuous incubation with these inhibitory agents over 5 days, a period during which processes become more complex and develop into multicellular cords, was somewhat less effective in inhibiting the morphogenetic activity (Fig. 4A and B right panels). While this suggests that the same set of factors (HGF and EGFR ligands) continues to play an important role in morphogenesis for up to 5 days, it also suggests that a significant fraction of the activity (\sim 50%) might not be accounted for by HGF and EGFR ligands.

A Number of Growth Factors Are Capable of Inducing *In Vitro* UB Cell Tubulogenesis. To more directly examine the role of HGF and EGFR ligands in UB cell tubulogenesis, and also to determine if other factors could be found that might account for the fraction of morphogenetic activity that could not be inhibited by the anti-HGF antibody and tyrphostin AG 1478, purified growth factors were added to the UB cells grown in type I collagen gels and compared with the effect of BSN-CM. [Collagen gels were employed because even growth factor-depleted Matrigel contains some remaining growth factor activity (16) that could complicate the interpretation.] During the initial 24–48 hr, several growth factors, including HGF, EGF, TGF- α , bFGF, and IGF-1, induced process formation of UB cells in three-dimensional culture (Fig. 5 Left; Table 1). GDNF, PDGF, and TGF- β 1 did not induce initial process formation (Fig. 5, Left; Table 1). BSN-CM induced UB cell processes which became more complex over several days, eventually forming multicellular cords (Fig. 3A; Table 1). However, while HGF, EGF, TGF- α , bFGF, and IGF-1 continued to induce complex processes for 2–3 days, after this time only high concentrations of IGF-1 and bFGF were able to sustain multicellular cords, though not nearly to the same degree as BSN-CM (Fig. 5 Right; Table 1). Moreover, a mixture of HGF, EGF, bFGF, IGF-1, and GDNF, which initially appeared as potent as BSN-CM, did not sustain complex multicellular structures (either cysts or cords) after 5–6 days of culture (Fig. 5; Table 1), and the “quality” and complexity of the structures induced by BSN-CM was clearly superior. In fact, only BSN-CM consistently induced branching tubular structures with clearly distinguishable lumens (Table 1).

DISCUSSION

We have established a system in which soluble factors from an apparently mesenchymal cell line (BSN) derived from the early embryonic kidney are able to induce branching tubulogenesis in a UB cell line in a three-dimensional ECM gel system. Only minimal amounts of serum were used. Thus, this represents perhaps the simplest system for the study of mesenchymal-epithelial interactions relevant to early kidney development.

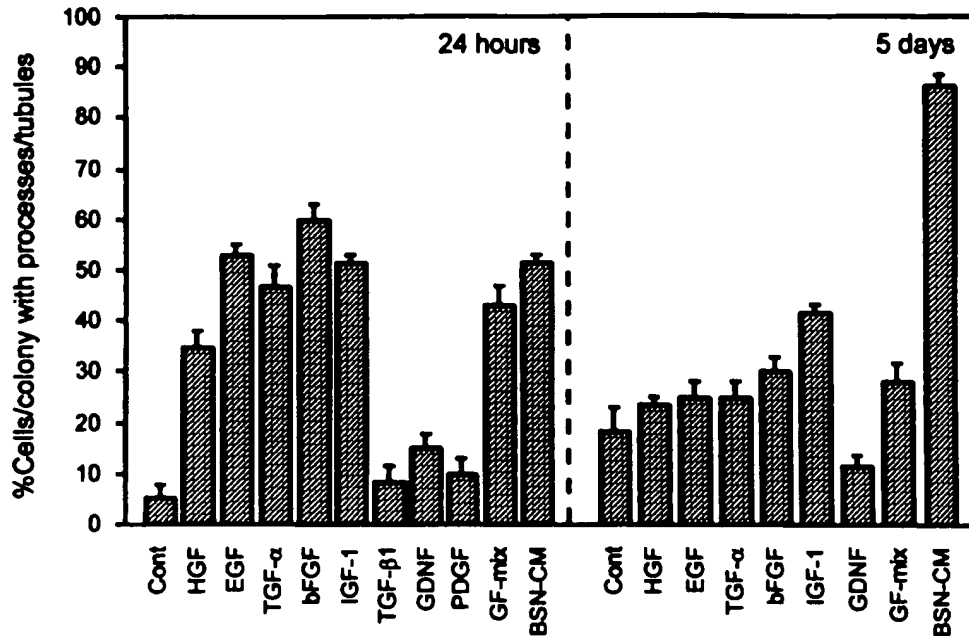


FIG. 5. BSN-CM maintains UB cell morphogenesis better than any other purified growth factor or their combination. Purified growth factors, a combination of growth factors (GF-mix: HGF, EGF, bFGF, IGF-1, and GDNF), or BSN-CM was applied on top of UB cells suspended in collagen gels. Tubulogenic activity was semiquantified by evaluating percentage of UB cells/colonies with processes/cords/tubules. At 24 hr of serum-free culture, HGF, EGF, TGF- α , bFGF, and IGF-1 were as capable of inducing UB cell processes as were GF-mix or BSN-CM medium. TGF- β 1, PDGF, and GDNF were not effective. At 5 days of culture (with 1% serum), only high concentrations of bFGF and IGF-1 could sustain the growth of UB cell processes into cord-like structures. BSN-CM was much more potent than any other growth factors listed or their combination. Statistical significance was determined and is presented in Table 1, where a qualitative analysis of structures is also presented.

Systems for branching tubulogenesis that have been employed previously utilize cell lines such as MDCK or mIMCD3 derived from the mature kidney (10–16, 36). In these cell lines, the major factors capable of inducing early cellular process formation leading to branching tubulogenesis appear to be HGF and EGFR ligands (e.g., EGF, TGF- α , heparin-binding EGF, amphiregulin, betacellulin) (10, 11). In contrast, the UB cells, apart from responding to HGF and EGFR ligands, also form

Table 1. Qualitative effect of growth factors on UB cell tubulogenesis

Growth factor	Process formation (24–48 hr)	Cord-like structure (5–6 days)	Tubules with lumen (>10 days)
HGF	+	±	–
EGF	+	–	–
TGF- α	+	–	–
bFGF	+	±	–
IGF-1	+	+	–
PDGF	–	ND	ND
GDNF	–	–	–
TGF- β 1	–	ND	ND
BSN-CM	+	+	+
GF-mix	+	+	–

Growth factors were applied on top of UB cell collagen gel suspension culture. Percentage of cells/colonies exhibiting tubules/processes was evaluated for each condition and compared to control condition (BSA or 1% FCS). If the specific growth factor treatment significantly increased tubulogenesis (i.e., $P < 0.05$ vs. control by unpaired Student's t test), the growth factor was marked +. If not, the growth factor was marked –. ± indicates variable result among experiments. ND, not done. Process and formation data were derived from five separate experiments, cord-like structure data were derived from three separate experiments. Tubules with lumen data were derived from two separate experiments. Only BSN-CM induced tubules with lumens. GF-mix contains HGF, EGF, bFGF, IGF-1, and GDNF.

processes in response to high concentrations of IGF-1 and bFGF (Fig. 5, Table 1). These growth factors can also induce the formation of multicellular cords in UB cells. Although a receptor for bFGF has been reported in the collecting duct (37), the fact that only high concentrations of bFGF induced UB cell tubulogenesis raises the possibility that this growth factor is not acting on classical bFGF receptors *per se*, but rather, on some other receptor that binds bFGF. However, neither alone nor in combination were these growth factors able to induce tubules with lumens. Only BSN-CM was capable of doing this (Table 1), suggesting that it contains additional growth factors capable of leading to the formation of branching tubules with lumens.

This raises an interesting question. Heretofore, the literature on *in vitro* tubulogenesis has been vague as to whether the phenomenon of tubule formation is simply the evolution of a single kind of process or whether multiple distinct steps are involved. Morphologically, there appear to be at least three clearly distinguishable morphogenetic events: the formation of cellular processes, the development into branching multicellular cords, and the establishment of tubules with lumens. Our data raise the possibility that these are distinct steps dependent on different sets of soluble factors. However, this issue probably cannot be clearly resolved until molecular markers specific for these steps are found, if indeed they are distinct, or relatively so.

Although perhaps somewhat less robust compared with the MDCK cell and mIMCD3 cell systems, the system we describe here may be viewed as a more authentic *in vitro* system for the study of branching tubulogenesis relevant to the developing kidney. Nevertheless, all these systems have potential limitations. The cell lines we have used express simian virus 40 antigen, and it is difficult to determine what effect this has on the behavior of the cells in the morphogenetic system. Nevertheless, the animals from which these cells were derived undergo apparently normal nephrogenesis with normal branching morphogenesis. It is also reassuring that coculturing

the embryonic kidney with the UB cells and incubating the UB cells with the conditioned medium from the BSN cells gave similar results (Fig. 4). Thus, in both cases, EGFR ligands and HGF accounted for the bulk of branching tubulogenic activity, but there was a significant fraction (≈ 40 –50%) of tubulogenic activity which could not be neutralized by the combination of neutralizing anti-HGF antibody and the specific EGFR antagonist. This was especially apparent in the long-term assays and is consistent with our finding that none of the growth factors we employed, individually or in combination, was capable of sustaining long-term morphogenesis leading to the formation of tubules with lumens. The nature of this additional factor remains to be determined. It is possible that this factor simply sustains tubular growth, thereby allowing other morphogens to act upon the developing multicellular structure, or that it functions as a true morphogen.

Although the UB cells express *c-ret*, at least by reverse transcription-polymerase chain reaction (25), we were unable to induce branching tubulogenesis with its ligand, GDNF (Fig. 5). This may be due to low levels of expression or the expression of a receptor that is not functionally active, at least in the context of the ECM gels we used. It is also conceivable that mesenchymal-epithelial cell contact is required for activation of the GDNF/*c-ret* axis.

Finally, while the BSN cells appear to be mesenchymal and exhibit clear-cut differences in marker profile from the UB cells (Fig. 1), it remains to be determined to what extent, if any, they themselves are capable of undergoing tubulogenesis and/or differentiating along the pathway leading to proximal tubule formation, as occurs in metanephric mesenchyme of the embryonic kidney. The fact that the BSN cells express *c-met* may suggest that, although largely mesenchymal in character, they have the potential for epithelialization or that they are at one of the earliest steps in this process. This constitutes an important area for future research.

This work was supported by a grant from the National Institute of Diabetes and Digestive and Kidney Diseases to S.K.N. This work was done during S.K.N.'s tenure as an Established Investigator of the American Heart Association. H.S. was supported by a Research Fellowship from the National Kidney Foundation. T.T. was supported in part by the Sandoz Foundation for Gerontological Research.

- Saxen, L. (1987) *Organogenesis of the Kidney* (Cambridge Univ. Press, Cambridge, U.K.).
- Nigam, S. K., Aperia, A. & Brenner, B. M. (1996) in *The Kidney*, ed: Brenner, B. M. (Saunders, Philadelphia), pp. 72–98.
- Stark, K., Vainio, S., Vassileva, G. & McMahon, A. P. (1994) *Nature (London)* **372**, 679–683.
- Luo, G., Hofmann, C., Bronckers, A. L., Sothocki, M., Bradley, A. & Karsenty, G. (1995) *Genes Dev.* **9**, 2808–2820.
- Dudley, A. T., Lyons, K. M. & Robertson, E. J. (1995) *Genes Dev.* **9**, 2795–2807.
- Santos, O. F., Barros, E. J., Yang, X. M., Matsumoto, K., Nakamura, T., Park, M. & Nigam, S. K. (1994) *Dev. Biol.* **163**, 525–529.
- Rogers, S. A., Ryan, G. & Hammerman, M. R. (1992) *Am. J. Physiol.* **262**, F533–F539.
- Rogers, S. A., Ryan, G. & Hammerman, M. R. (1991) *J. Cell Biol.* **113**, 1447–1453.
- Liu, Z. Z., Kumar, A., Wallner, E. I., Wada, J., Carone, F. A. & Kanwar, Y. S. (1994) *Eur. J. Cell Biol.* **65**, 378–391.
- Barros, E. J., Santos, O. F., Matsumoto, K., Nakamura, T. & Nigam, S. K. (1995) *Proc. Natl. Acad. Sci. USA* **92**, 4412–4416.
- Cantley, L. G., Barros, E. J., Gandhi, M., Rauchman, M. & Nigam, S. K. (1994) *Am. J. Physiol.* **267**, F271–F280.
- Derman, M. P., Cunha, M. J., Barros, E. J., Nigam, S. K. & Cantley, L. G. (1995) *Am. J. Physiol.* **268**, F1211–F1217.
- Montesano, R., Schaller, G. & Orci, L. (1991) *Cell* **66**, 697–711.
- Sakurai, H. & Nigam, S. K. (1997) *Am. J. Physiol.* **272**, F139–F146.
- Santos, O. F., Moura, L. A., Rosen, E. M. & Nigam, S. K. (1993) *Dev. Biol.* **159**, 535–548.
- Santos, O. F. & Nigam, S. K. (1993) *Dev. Biol.* **160**, 293–302.
- Rosen, E. M., Nigam, S. K. & Goldberg, I. D. (1994) *J. Cell Biol.* **127**, 1783–1787.
- Stuart, R. O., Barros, E. J., Ribeiro, E. & Nigam, S. K. (1995) *J. Am. Soc. Nephrol.* **6**, 1151–1159.
- Nigam, S. K. (1995) *Curr. Opin. Nephrol. Hypertension* **4**, 209–214.
- Bladt, F., Riethmacher, D., Isenmann, S., Aguzzi, A. & Birchmeier, C. (1995) *Nature (London)* **376**, 768–771.
- Schmidt, C., Bladt, F., Goedecke, S., Brinkmann, V., Zschiesche, W., Sharpe, M., Gherardi, E. & Birchmeier, C. (1995) *Nature (London)* **373**, 699–702.
- Uehara, Y., Minowa, O., Mori, C., Shiota, K., Kuno, J., Noda, T. & Kitamura, N. (1995) *Nature (London)* **373**, 702–705.
- Luetteke, N. C., Qui, T. H., Peiffer, R. L., Oliver, P., Smithies, O. & Lee, D. C. (1993) *Cell* **73**, 263–278.
- Mann, G. B., Fowler, K. J., Gabriel, A., Nice, E. C., Williams, R. L. & Dunn, A. R. (1993) *Cell* **73**, 249–261.
- Barasch, J., Pressler, L., Connor, J. & Malik, A. (1996) *Am. J. Physiol.* **271**, F50–F61.
- Palmiter, R. D., Chen, H. Y., Messing, A. & Brinster, R. L. (1985) *Nature (London)* **316**, 457–460.
- Rauchman, M. I., Nigam, S. K., Delpire, E. & Gullans, S. R. (1993) *Am. J. Physiol.* **265**, F416–F424.
- Bush, K. T., Stuart, R. O., Li, S.-H., Moura, L. A., Sharp, A. H., Ross, C. A. & Nigam, S. K. (1994) *J. Biol. Chem.* **269**, 23694–23699.
- Kuznetsov, G., Chen, L. B. & Nigam, S. K. (1997) *J. Biol. Chem.* **272**, 3057–3063.
- Chomczynski, P. & Sacchi, N. (1987) *Anal. Biochem.* **162**, 156–159.
- Howarth, A. G., Hughes, M. R. & Stevenson, B. R. (1992) *Am. J. Physiol.* **262**, C461–C469.
- Karp, S. L., Ortiz-Arduan, A., Li, S. & Neilson, E. G. (1994) *Proc. Natl. Acad. Sci. USA* **91**, 5286–5290.
- Sonnenberg, E., Meyer, D., Weidner, K. M. & Birchmeier, C. (1993) *J. Cell Biol.* **123**, 223–235.
- Fry, D. W., Kraker, A. J., McMichael, A., Ambrosio, L. A., Nelson, J. M., Leopold, W. R., Connors, R. W. & Bridges, A. J. (1994) *Science* **265**, 1093–1095.
- Levitzi, A. & Gazit, A. (1995) *Science* **267**, 1782–1788.
- Montesano, R., Matsumoto, K., Nakamura, T. & Orci, L. (1991) *Cell* **67**, 901–908.
- Wanaka, A., Milbrandt, J. & Johanson, E. M., Jr. (1991) *Development (Cambridge, U.K.)* **111**, 455–468.

Analysis of affinity and structural selectivity in the binding of proteins to glycosaminoglycans: Development of a sensitive electrophoretic approach

MATTHIAS K. LEE* AND ARTHUR D. LANDER*†‡

*Department of Biology and †Department of Brain and Cognitive Sciences, Massachusetts Institute of Technology, Cambridge, MA 02139

Communicated by Phillip A. Sharp, December 13, 1990

ABSTRACT Members of several families of cell surface and secreted proteins bind glycosaminoglycans (GAGs), the structurally heterogeneous polysaccharides found on proteoglycans. To understand the physiological significance of the interactions of proteins with GAGs, it is critical that relationships between GAG structure and binding be analyzed. It is particularly important that interactions depending on common structural features of GAGs (e.g., size, charge density, and disaccharide repeat unit) be distinguished from those mediated by specific sequences of carbohydrate modification. Gathering the information needed to make such distinctions has so far been difficult, however, partly because structurally homogeneous samples of GAGs are lacking but also because of technical difficulties associated with performing and interpreting assays of protein–GAG binding. We describe an electrophoretic method useful for both measuring affinity and evaluating structural selectivity in protein–GAG binding. Data are presented on the binding of the GAG heparin to the protease inhibitor antithrombin III, the acidic and basic fibroblast growth factors, and the extracellular matrix protein fibronectin. Results obtained with fibronectin are consistent with a model in which high-affinity binding ($K_d \approx 34$ nM) is mediated through the recognition of specific carbohydrate sequences.

Proteins that bind glycosaminoglycans (GAGs) include many cell adhesion molecules, glycoproteins of the extracellular matrix, polypeptide growth factors, secreted proteases and antiproteases, and proteins involved in lipoprotein uptake (1, 2). In the tissue environments in which these proteins are found, GAGs are present as side chains of proteoglycans and exhibit diversity in length, disaccharide composition, and patterns of N- and O-sulfation.

For most GAG-binding proteins, the relationship between GAG structure and binding affinity is poorly understood. For some, all that is known is that a high concentration of salt is required to elute them from heparin-agarose columns; sometimes the relative abilities of GAGs of different classes (e.g., heparan sulfate, chondroitin sulfate, dermatan sulfate, keratan sulfate, etc.) to compete away such binding has also been measured (e.g., refs. 3 and 4). Those direct measurements of affinity that have been made have often required derivatization or immobilization of either protein or GAG (e.g., refs. 5–7); such measures may inhibit (e.g., by blocking sites of interaction) or artificially enhance (e.g., by favoring multivalent interactions) binding. Quantifying binding is also impeded by the fact that most GAG–protein K_d values are thought to be in the range of 5–500 nM, where the possibility of rapid dissociation kinetics argues against the use of many types of binding assays that involve separation and washing of bound complexes. In addition, measurements that have been made of GAG–protein affinity have usually measured

the average affinity of a protein for the structurally heterogeneous set of binding sites represented by any GAG sample. Selectivity of a protein for specific sequences of carbohydrate modification is, therefore, not readily appreciated, despite the fact that such selectivity exists and is, in at least one case, of considerable physiological importance (8).

Below, experiments are presented in which the principle of affinity electrophoresis (9) was exploited to analyze protein–GAG binding. The technique described is referred to as affinity coelectrophoresis (ACE) because both protein and GAG are permitted to migrate freely during electrophoresis (typically, in affinity electrophoresis, as in affinity chromatography, one ligand is physically immobilized). The method uses small amounts of material and can yield values of the affinity constant even when dissociation is rapid (e.g., when affinity is low). Experiments are presented in which ACE was used to identify and isolate a subpopulation of heparin molecules to which fibronectin binds selectively. Some of these data have been presented in abstract form (10, 11).

MATERIALS AND METHODS

Materials. Low-melting-point agarose (SeaPlaque) and GelBond were purchased from FMC, heparin (grade I, from porcine intestinal mucosa) was from Sigma, chondroitin sulfate (from shark cartilage) was from Fluka, bovine serum albumin (crystalline) was from ICN, and human plasma fibronectin (FN) was from New York Blood Center (New York). Basic fibroblast growth factor (bFGF) and acidic fibroblast growth factor (aFGF) were purified from bovine brain (12). Human antithrombin III (AT) was the generous gift of Robert Rosenberg (M.I.T.). β -Nerve growth factor was generously donated by Randall Pittman (University of Pennsylvania).

Heparin was substituted with fluoresceinamine to a level of 15.7 ng/ μ g (13) and radioiodinated to a specific activity of 110,000 cpm/ng (14). A portion of the 125 I-labeled fluoresceinamine-heparin (125 I-F-heparin) was fractionated by gel filtration [on Sephadex G-100 in 50 mM sodium 3-(*N*-morpholino)-2-hydroxypropanesulfonate (Mopso), pH 7.0/125 mM sodium acetate] and the last 10.8% of the radioactive material to elute ($0.57 < K_{av} < 0.76$) was pooled as a low molecular weight (LMW) fraction. This fraction was estimated to contain heparin chains of $M_r \leq 6000$ (3, 15–18).

Electrophoretic Analysis of Binding. Low-melting-point agarose (1%) was prepared in either of two electrophoresis buffers: 50 mM sodium Mopso, pH 7.0/125 mM sodium acetate/0.5% 3-[(3-cholamidopropyl)dimethylammonio]-1-

Abbreviations: ACE, affinity coelectrophoresis; aFGF and bFGF, acidic and basic fibroblast growth factor, respectively; AT, antithrombin III; CHAPS, 3-[(3-cholamidopropyl)dimethylammonio]-1-propanesulfonate; 125 I-F-heparin, 125 I-labeled fluoresceinamine-heparin; FN, fibronectin; GAG, glycosaminoglycan; LMW, low molecular weight; Mopso, 3-(*N*-morpholino)-2-hydroxypropanesulfonic acid.

‡To whom reprint requests should be addressed.

The publication costs of this article were defrayed in part by page charge payment. This article must therefore be hereby marked "advertisement" in accordance with 18 U.S.C. §1734 solely to indicate this fact.



FIG. 1. Schematic representation of a gel before and after electrophoresis. Proteins are cast at various concentrations into nine rectangular zones within an agarose gel (A); the dark line at top represents a slot into which labeled GAG is introduced. During electrophoresis, GAGs migrate through the rectangular zones but are slowed by binding to proteins. This produces a series of peaks (B), from which an affinity constant may be derived (see text).

propanesulfonate (CHAPS) (buffer A) or 50 mM sodium Mopso, pH 7.0/125 mM NaCl/0.5% CHAPS (buffer B). A Teflon comb consisting of nine parallel bars, each $45 \times 4 \times 4$ mm and held rigidly together with a spacing of 3 mm between bars, was placed onto GelBond film fitted to a Plexiglas casting tray (75×100 mm) with the long axis of the bars parallel to the long dimension of the tray. A Teflon strip ($66 \times 37 \times 1$ mm) was stood on edge with its long dimension parallel to the short dimension of the casting tray, at a distance of 4 mm from one edge of the Teflon comb. Tabs extending from the Teflon strip enabled it to be held upright by tape affixed to the casting tray. Typically, 19 ml of agarose were poured hot ($>70^\circ\text{C}$) to achieve a cooled gel ≈ 4 mm thick. Removal of the comb and strip resulted in a gel containing nine 4×45 mm rectangular wells adjacent to a 66×1 mm slot (Fig. 1A).

Protein samples (typically 350 μl) were prepared in electrophoresis buffer at twice the desired concentrations. Samples were mixed with an equal volume of melted 2% (wt/vol) agarose at 37°C , pipetted into the appropriate rectangular wells, and allowed to gel. After submerging a protein-loaded gel in the electrophoresis chamber (Hoefer SuperSub) containing buffer minus CHAPS, ≈ 190 μl of ^{125}I -F-heparin [4 ng/ml in electrophoresis buffer containing 0.5% bromphenol blue and 6% (wt/vol) sucrose] was added to the 66×1 mm slot.

Typically, electrophoresis was performed at 60–70 V (2–2.4 V/cm) for 0.75–2 hr, with currents of ≈ 330 mA (in buffer A). Buffer was recirculated, and a flow of cold tap water through the coolant ports of the apparatus was used to maintain buffer temperature at 20 – 25°C . Endpoints were determined by the position of the bromphenol blue, which migrated about half as rapidly as heparin. Gels were air-dried and autoradiographed against preflashed film at -80°C . In some experiments, ^{125}I -F-heparin was recovered from gels by electroelution in 0.75 mM NaOAc/0.25 mM sodium Mopso,

pH 7, concentrated 2-fold using a SpeedVac evaporator (Savant), and retested for binding using ACE.

RESULTS

Demonstration of Protein–GAG Binding. At neutral pH, the electrophoretic mobilities of most proteins are much lower than those of GAGs. Consequently, the binding of proteins to GAGs should, in most cases, retard GAG electrophoresis. To determine whether this effect could be exploited to quantify protein–GAG binding, a method was devised for electrophoresing labeled GAGs through zones containing multiple protein samples. Briefly, special combs were used to create agarose gels of the configuration shown in Fig. 1A. The long rectangles represent wells into which proteins in molten low-gelling-temperature agarose (at 37°C) could be introduced and allowed to gel. The dark line at the top of Fig. 1A indicates where samples of labeled GAGs were introduced. The position of the anode is at the bottom. Fig. 1B presents the expected experimental results when the nine wells contain a single GAG-binding protein at a series of concentrations decreasing from left to right: at sufficiently high protein concentrations, migration of the GAG front (thick black line) is retarded in a dose-dependent manner. The protein-free spaces between the wells facilitate measurement of the changes in mobility associated with each protein concentration.

Fig. 2A shows that the predicted pattern was indeed obtained when ^{125}I -F-heparin was electrophoresed at neutral pH and physiological ionic strength through zones containing a known heparin-binding protein, bFGF. In response to bFGF concentrations of up to 35 nM, heparin mobility was reduced up to 88%. The effect was specific, in that even much higher concentrations of nerve growth factor (a protein of similar size and isoelectric point to bFGF) had no effect on ^{125}I -F-heparin mobility (Fig. 2B).

An assumption made in predicting the simple pattern shown in Fig. 1B was that all heparin molecules behave more or less identically. The data in Fig. 2A and B support this assumption. In contrast, experiments performed with a different heparin-binding protein, AT, illustrate the type of pattern that can result when heparin molecules do not behave identically (Fig. 2C). In this case, the migrating heparin front was split by AT into two distinct fronts, one of which was progressively slowed by AT concentrations ≥ 5 nM, whereas the other was shifted only slightly by AT at 1 μM . The same result was obtained with a size-selected LMW fraction of ^{125}I -F-heparin (Fig. 2D). A large excess of unlabeled heparin

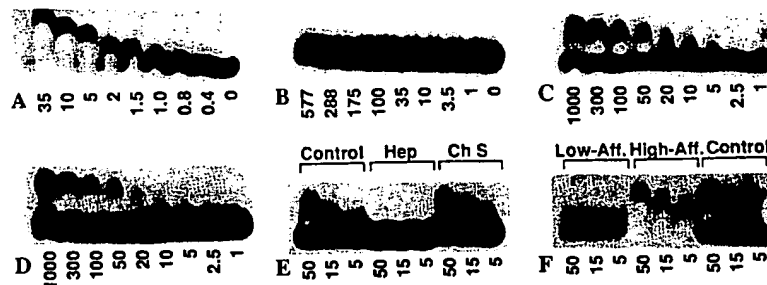


FIG. 2. (A–D) Autoradiographs of gels in which ^{125}I -F-heparin was electrophoresed through zones containing bFGF (A), β -nerve growth factor (B), and AT (C and D). Protein concentrations are in nM. (B and D) Size-selected LMW heparin was used. (E) Inhibition of binding of ^{125}I -F-heparin to AT by unlabeled heparin. In this experiment, a gel was cast with three sample slots, each opposite three of nine rectangular zones. Equal amounts of ^{125}I -F-heparin were introduced into each slot. In the central slot, unlabeled heparin (1 mg/ml) was mixed with the labeled sample; in the slot at right, unlabeled chondroitin sulfate (1 mg/ml) was added. Concentrations of AT are in nM. (F) Recovery and analysis of heparin with high and low affinity for AT. A set of three sample slots was prepared as in E. Into the slot at left was loaded material isolated from LMW ^{125}I -F-heparin that had previously migrated through AT-containing agarose without retardation (lanes Low-Aff.). Material that had been retarded by AT was isolated and loaded in the central slot (lanes High-Aff.). Control ^{125}I -F-heparin was loaded in the slot at right. Concentrations of AT are shown in nM.

readily blocked the effects of AT on heparin mobility, but an equal concentration of chondroitin sulfate did not (Fig. 2E).

These results fit with what is known about the properties of AT, one of the most studied GAG-binding proteins: AT binds a subset of heparin molecules, with subtleties of carbohydrate sequence, rather than heparin chain length, providing the basis for selectivity (19). To confirm that the two heparin fronts observed in ACE gels containing AT actually result from the fractionation of heparin into distinct species with different binding properties, a gel similar to the one shown in Fig. 2D was electrophoresed and pieces of agarose were cut out of locations where the two heparin fronts were well separated. The pieces were then melted, and their contents were retested for binding to AT. The results (Fig. 2F) confirm that separable fractions of heparin account for the pattern in Fig. 2D.

Measurement of Binding Affinity. In general, heparin's mobility in any protein-containing environment should be the average of the mobilities of protein-bound heparin and free heparin, weighted according to the fraction of time that heparin molecules spend in the bound and free states. To quantify protein-induced shifts in mobility, it is convenient to introduce a unitless number, the retardation coefficient R ($R = (M_0 - M)/M_0$, where M_0 is the mobility of free heparin and M is heparin's observed mobility through a protein-containing zone). Provided that heparin and protein form a 1:1 complex, R at any protein concentration should be proportional to the amount of heparin bound. Moreover, if R_∞ is taken to represent the value of R seen at full saturation (i.e., at an arbitrarily high concentration of binding protein), then R/R_∞ should be equivalent to the fractional saturation. Accordingly, experimental values of R should vary with protein concentration according to the Scatchard equation; specifically, a plot of $R/[\text{protein}]_{\text{free}}$ vs. R should yield a straight line with a slope of $-1/K_d$ and a y intercept of R_∞/K_d . If the concentration of heparin is small compared to K_d , plotting $R/[\text{protein}]_{\text{total}}$ vs. R should yield the same plot.

Two such plots are shown in Fig. 3. The data for bFGF binding to LMW heparin (Fig. 2A) fit a line implying a K_d of 2 nM. For AT binding to LMW heparin, values of R obtained from Fig. 2D also fit a line, implying a K_d of 16 nM (Fig. 3B). Straight lines also fit the data obtained for the binding of unfractionated heparin to bFGF and AT, and for the binding of heparin to aFGF and serum albumin (data not shown). These findings are summarized in Table 1. Results with two buffer systems that differed in their major anion (chloride vs. acetate) did not differ significantly.

Characterization of Heparin Binding to FN. FN is a major glycoprotein of the extracellular matrix and a component of plasma (20, 21). FN binds heparin and heparan sulfate (3, 22, 23), whereupon alterations in its structural properties and ability to bind other molecules can be detected (e.g., refs. 24–26). Recent evidence indicates that the attachment of epithelial cells and fibroblasts to FN is mediated, in part, by cell surface heparan sulfate (27, 28).

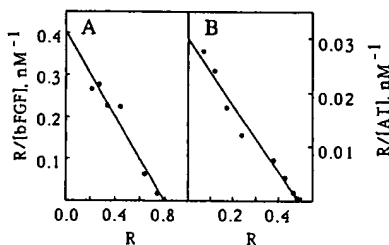


FIG. 3. Graphic analysis of binding of bFGF to LMW heparin (A) and binding of AT to the high-affinity fraction of LMW heparin (B). The lines drawn imply K_d values of 2 nM for bFGF and 16 nM for AT.

Plasma FN, a disulfide-linked dimer, is eluted from heparin-Sepharose between 0.3 and 0.5 M NaCl (29). Two distinct heparin-binding fragments of FN have been identified and mapped. Yamada *et al.* (3) used a filter-binding assay to measure the binding of [³H]heparin to FN and obtained a biphasic Scatchard plot, suggestive of two component affinities (K_d values of 4.2 nM and 110 nM), but were unable to determine whether their data reflected differences in the affinity of heparin for two distinct sites on FN or the presence of subspecies of heparin that bind FN with different affinities. In addition, values of K_d were derived assuming that heparin molecules contain only one binding site for FN. This assumption may not be valid, especially given that particularly long heparin chains (average M_r , 12,000) were used in that study (3).

Analysis of the heparin–FN interaction by ACE is shown in Fig. 4A. At high FN concentrations, LMW ¹²⁵I-F-heparin was observed to shift to a single very low mobility, implying that essentially all heparin molecules bind FN. At somewhat lower FN concentrations, however, the labeled material migrated not as a discrete band but as a diffuse smear. It seemed likely that this smear represented the fractionation of individual heparin molecules according to differences in affinity for FN.

To test this possibility, LMW ¹²⁵I-F-heparin was electrophoresed through a single zone of 125 nM FN. The gel was then cut transversely into segments, and fractions were pooled representing the leading 26% of the ¹²⁵I-F-heparin (pool 1, "weakly retarded heparin") and the trailing 26% (pool 2, "strongly retarded heparin"). The samples were heated to 100°C for 10 min (to denature FN) and labeled heparin was recovered by electroelution. The resulting material was retested for binding to FN. As shown in Fig. 4B and C, the ACE patterns for pools 1 and 2 were distinctly different from each other and considerably less diffuse than those of the starting material.

Graphical analysis of the patterns in Fig. 4B and C is shown in Fig. 5. The data from pool 1 yield a linear plot, suggesting a K_d of 640 nM. Pool 2 yields an apparently discontinuous plot—two line segments with similar slopes (implying K_d values of 32 and 36 nM). Examination of Fig. 4C indicates how the result for pool 2 arises: with increasing FN concentration, heparin's mobility decreases, levels off at $R \approx 0.5$,

Table 1. Measurement of protein affinities for heparin and LMW heparin

Protein	Heparin	K_d , nM
bFGF	Unfractionated	2.2
	LMW	2.0
	LMW	3.1*
AT	Unfractionated, HA	11
	LMW, HA	16
	LMW, HA	12*
	Unfractionated, LA†	~6000
aFGF	LMW	91
Plasma FN	LMW, HA‡	34
	LMW, LA‡	640
Nerve growth factor	LMW	>600§
Serum albumin	LMW	4300

Measurements were made in buffer A except for those indicated by an asterisk, which were made in buffer B. HA and LA refer to strongly retarded (high affinity) and weakly retarded (low affinity) fractions, respectively, as isolated from ACE gels (see text). As described in the Discussion, correct values of K_d for bFGF may be lower by as much as 0.8 nM.

†Estimated from data in Fig. 2C and the assumption that R_∞ for low-affinity heparin will be the same as that observed for high-affinity heparin.

‡From the experiment described in Figs. 4 and 5.

§Highest concentration tested.

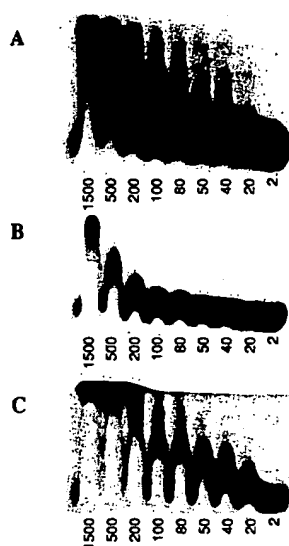


FIG. 4. Analysis of heparin-FN binding. (A) Electrophoresis of ^{125}I -F-heparin through zones containing FN (concentrations in nM, based on a molecular weight of 440,000). In contrast to the examples in Fig. 1, the migrating heparin front becomes broadly smeared at protein concentrations between 50 and 500 nM. (B and C) After electrophoresis of ^{125}I -F-heparin in the presence of 125 nM FN, the 26% of labeled material that was retarded least (pool 1) and the 26% of labeled material that was retarded most (pool 2) were recovered by electroelution and retested for binding to FN. The patterns produced by pool 1 (B) and pool 2 (C) are distinctly different.

and then shifts again, leveling off at $R \approx 0.8$. This behavior is most easily explained by the known tendency of FN to self-aggregate when concentrated (see ref. 30). Thus, the first shift (to $R \approx 0.5$) may represent saturation of heparin by single FN molecules, whereas the second shift (to $R \approx 0.8$) reflects aggregation of FN molecules into oligomers (which, being larger, more strongly retard heparin's mobility). In support of this view, studies in which trace amounts of ^{125}I -labeled FN were electrophoresed in the presence of unlabeled FN showed that the mobility of FN in 2% agarose undergoes a concentration-dependent decrease (consistent with aggregation) in the expected range (10–200 nM) (unpublished observations).

Thus the data in Figs. 4 and 5 indicate that LMW heparin is heterogeneous and that classes of heparin molecules that differ by as much as 20-fold in affinity for FN can be isolated. To test whether this difference in affinity depends on heparin size (chain length), pools 1 and 2 were compared by gel

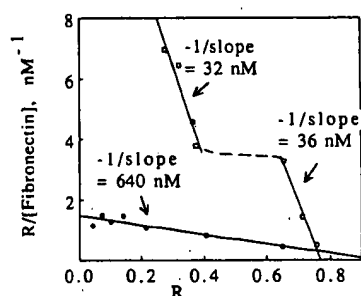


FIG. 5. Graphic analysis of data in Fig. 4 B and C. Weakly retarded heparin (●) yields a linear plot implying a K_d value of 640 nM. Strongly retarded heparin (□) yields a discontinuous plot with two line segments that imply K_d values of 32 nM and 36 nM. The discontinuity apparently reflects oligomerization of FN at high concentrations (see text).

filtration on Sephadex G-75 in 10 mM Mopso, pH 7.0/125 mM sodium acetate/4 M urea. The size distributions of molecules in pools 1 and 2 were largely overlapping, with those of pool 1 being slightly smaller ($K_{av} = 0.250$) and those in pool 2 slightly larger ($K_{av} = 0.162$) than the LMW heparin from which both pools were derived ($K_{av} = 0.235$) (data not shown). To assess whether the molecules in pools 1 and 2 differed greatly in charge density (a reflection of the degree of sulfation), their electrophoretic mobilities in 1% agarose (containing no binding proteins) were compared. The mobilities obtained for the two pools were identical: $5.6 \pm 0.03 \times 10^{-8} \text{ m}^2/\text{V}\cdot\text{s}$ for pool 1 and $5.6 \pm 0.05 \times 10^{-8} \text{ m}^2/\text{V}\cdot\text{s}$ for pool 2 (in buffer A at 25°C).

DISCUSSION

We report here the development of an affinity-electrophoretic technique, ACE, for studying GAG-protein interactions. Binding is measured at physiological pH and ionic strength and under conditions in which interacting molecules are freely mobile. ACE can in principle be used to measure binding between any two macromolecules, provided that the complex they form has an electrophoretic mobility different from that of at least one of its components. In practice, this difference should be large enough that distances migrated by bound and free ligand are distinguishable within reasonable time. In some of the experiments described above, it was possible to achieve sufficient separations with electrophoresis of the GAG front through only 20 mm of gel; in no experiment was electrophoresis through >50 mm necessary. These distances required short electrophoresis times at modest field strengths (e.g., 2.4 V/cm for 1–2 hr). Also, because electrophoresis was carried out in a gel of small width and height, little material was required. For example, to measure binding of heparin to AT in Fig. 2E, only 400 pmol of protein and 75 fmol of GAG were used. Considering that ACE can measure affinities when dissociation rates are fast and that other techniques for doing so [e.g., equilibrium gel filtration (31, 32)] can require large amounts of material, the sensitivity of ACE seems particularly good.

Accurate determination of affinity constants using ACE requires that the following conditions be met. (i) The radio-labeling of one component should not affect binding. (ii) The physical properties of the gel should not affect binding. (iii) The kinetics of association and dissociation should be rapid compared to the time of electrophoresis. In the experiments reported here, heparin was substituted with <1 fluorescein-amine per molecule and radioiodinated (14); the possibility that labeling interfered with binding is argued against by ACE experiments on the binding of intact proteoglycans (labeled by protein radioiodination) to FN and the binding of heparan sulfate (metabolically labeled) to AT, which have yielded results similar to those reported here (ref. 11; T. Kojima, G. Marchildon, and R. Rosenberg, personal communication). Also, electrophoresis was performed using a highly porous matrix (1% agarose) to minimize effects of sieving on molecular interactions, and electrophoresis times were long (1–2 hr) compared with likely kinetic constants.

As shown in Figs. 3 and 5, it is convenient to analyze ACE data by plotting $R/[\text{protein}]_{\text{total}}$ vs. R and to obtain an apparent value of K_d from the slope. Strict validity of this procedure has the following three requirements.

(i) **Concentration of GAG Is Much Less Than the K_d .** Use of the total, rather than the free, concentration of protein in the Scatchard equation is convenient, because it does not require the concentration of labeled heparin to be known accurately. This substitution is valid as long as the total concentration of heparin is sufficiently low. Otherwise, deviations from linearity at low values of R will occur, leading to a possible overestimation of K_d (by an amount no greater than the heparin concentration itself). The results in Table 1 were

obtained using heparin at 4 ng/ml, which for LMW heparin chains (estimated M_r , 5000–6000) is equivalent to 0.7–0.8 nM (for unfractionated heparin, the molar concentration would be lower). At this heparin concentration, the K_d values in Table 1 should be reasonably accurate with one exception: For the binding of bFGF to LMW heparin, the measured K_d of 2.0–3.1 nM should probably be revised to 1.2–2.4 nM.

(ii) **Mobilities of GAG-Protein Complexes Are Independent of Protein Concentration.** The assertion that the retardation coefficient R is proportional to the fractional saturation of GAG by protein assumes that the GAG-protein complex has a single fixed mobility. In some cases this may not be true, as results obtained with FN illustrate. Because of protein-protein interactions, mobility of the heparin-FN complex is lower at high FN concentrations than at low FN concentrations, giving rise to a nonlinear Scatchard plot (Fig. 5).

(iii) **GAGs Are Not Multivalent.** The binding of a second (or third, etc.) protein molecule to a GAG is not likely to produce as large a change in mobility as the binding of the first. Accordingly, if GAGs are multivalent, ACE data will tend to emphasize the behavior of the first site to saturate. If multiple sites of equivalent affinity are present, the Scatchard plots obtained may, for statistical reasons, be nonlinear and possess slopes that lead to an underestimation of the intrinsic K_d of the binding sites (by a factor not exceeding the number of binding sites). A more detailed treatment of the effects of multivalency and protein-protein interactions on ACE patterns will be presented elsewhere (unpublished results).

In this study, measurements were made of the affinity of several proteins for heparin. Where prior information on affinity is available, it agrees reasonably well with the results presented here. For example, affinity chromatographic studies of heparin binding to AT indicate that two populations of heparin exist, one with high affinity and one with low affinity, and that the latter species is more abundant in commercial preparations of heparin (8, 33); the data in Fig. 2 E and F imply both of these statements. The K_d values reported in Table 1 for the binding of heparin to AT are within or close to the range of values that have been published by others, namely, 12.5–100 nM for the high-affinity fraction of heparin and 20–100 μ M for the low-affinity fraction (5, 8, 16). Methodological differences or differences in the ionic composition of buffers may account for the ranges of values.

For bFGF, the values in Table 1 agree reasonably well with affinities reported for the binding of this growth factor to cell surface heparan sulfate, namely, 0.5 nM (34) and 2 nM (35), especially if the values in Table 1 are corrected as described above. The affinity of 91 nM obtained with aFGF is consistent with the fact that the binding of this growth factor to heparin-agarose is apparently weaker than that of bFGF (36).

For FN binding to heparin, ACE analysis uncovered evidence of selective binding of FN to subpopulations of heparin molecules. Although classes exhibiting two distinct K_d values were identified, they were derived from the 52% of heparin molecules that were either most strongly or most weakly retarded; therefore, it is possible that molecules with intermediate affinities were also present. When heparin subpopulations binding strongly and weakly to FN were compared, no difference in overall charge density was detected. Strongly binding heparin molecules were, however, slightly larger on average than weakly binding ones. These are precisely the properties expected if high-affinity binding to fibronectin is mediated by one or more specific rare carbohydrate sequences. A slightly larger size for high-affinity molecules is predicted on statistical grounds, as rare sequences are expected to be most common on long chains (15). Indeed, the same phenomenon has been observed with AT: fractionation of heparin populations by their affinity for AT produces a high-affinity fraction with an average size slightly larger than the low-affinity fraction (15, 16) despite the fact

that the binding of AT is mediated by a specific short carbohydrate sequence (19).

If, as the data presented here suggest, FN recognizes specific carbohydrate sequences on heparin, it will be important to investigate the binding of FN to heparan sulfates, which bear the same carbohydrate modifications as heparin but which are widely distributed *in vivo*. Interestingly, large differences have been reported in the degree to which heparan sulfates from different sources bind FN (e.g., refs. 3 and 37). These results raise the possibility that cells, by controlling specific steps in GAG modification, could modulate their ability to use heparan sulfate as a cell-surface receptor for FN (27, 28).

We thank Dr. R. Rosenberg (M.I.T.) for many helpful discussions during the development of this method and for the generous gift of AT. This work was supported by National Institutes of Health Grant NS26862. M.K.L. was supported in part by the Undergraduate Research Opportunities Program of M.I.T.

1. Lindahl, U. & Hook, M. (1978) *Annu. Rev. Biochem.* **47**, 385–417.
2. Jackson, R. L., Busch, S. J. & Cardin, A. D. (1991) *Physiol. Rev.* **71**, 481–539.
3. Yamada, K. M., Kennedy, D. W., Kimata, K. & Pratt, R. M. (1980) *J. Biol. Chem.* **255**, 6055–6063.
4. Del Rosso, M., Cappalletti, R., Viti, M., Vannucchi, S. & Chiarugi, V. (1981) *Biochem. J.* **199**, 699–704.
5. Rosenberg, R. D., Oosta, G. M., Jordan, R. E. & Gardner, W. T. (1980) *Biochem. Biophys. Res. Commun.* **96**, 1200–1208.
6. Jordan, R. E., Oosta, G. M., Gardner, W. T. & Rosenberg, R. D. (1980) *J. Biol. Chem.* **255**, 10073–10080.
7. Skubitz, A. P. N., McCarthy, J. B., Charonis, A. S. & Furcht, L. T. (1988) *J. Biol. Chem.* **263**, 4861–4868.
8. Bjork, I. & Lindahl, U. (1982) *Mol. Cell. Biochem.* **48**, 161–182.
9. Horejsi, V. (1981) *Anal. Biochem.* **112**, 1–8.
10. Lee, M. K. & Lander, A. D. (1989) *J. Cell Biol.* **109**, 109 (abstr.).
11. Herndon, M. E., Lee, M. K. & Lander, A. D. (1990) *J. Cell Biol.* **111**, 267 (abstr.).
12. Lobb, R. R. & Fett, J. W. (1984) *Biochemistry* **23**, 6295–6299.
13. Glabe, C. G., Harty, P. K. & Rosen, S. D. (1983) *Anal. Biochem.* **130**, 287–294.
14. Smith, J. W. & Knauer, D. J. (1987) *Anal. Biochem.* **160**, 105–114.
15. Laurent, T. C., Tengblad, A., Thunberg, L., Hook, M. & Lindahl, U. (1978) *Biochem. J.* **175**, 691–701.
16. Jordan, R., Beeler, D. & Rosenberg, R. (1979) *J. Biol. Chem.* **254**, 2902–2913.
17. Rosenberg, R. D., Jordan, R. E., Favreau, L. V. & Lam, L. H. (1979) *Biochem. Biophys. Res. Commun.* **86**, 1319–1324.
18. Danielsson, A. & Bjork, I. (1981) *Biochem. J.* **193**, 427–433.
19. Lindahl, U., Thunberg, L., Backstrom, G., Riesenfeld, J., Norling, K. & Bjork, I. (1984) *J. Biol. Chem.* **259**, 12368–12376.
20. Hynes, R. O. (1985) *Annu. Rev. Cell Biol.* **25**, 295–305.
21. Ruoslahti, E. (1988) *Annu. Rev. Biochem.* **57**, 375–413.
22. Ruoslahti, E. & Engvall, E. (1980) *Biochim. Biophys. Acta* **631**, 350–358.
23. Stamatoglou, S. C. & Keller, J. M. (1982) *Biochim. Biophys. Acta* **719**, 90–97.
24. Welsh, E. J., Frangou, S. A., Morris, E. R., Rees, D. A. & Chavin, S. I. (1983) *Biopolymers* **22**, 821–831.
25. Osterlund, E., Eronen, I., Osterlund, K. & Vuento, M. (1985) *Biochemistry* **24**, 2661–2667.
26. Johansson, S. & Hook, M. (1980) *Biochem. J.* **187**, 521–524.
27. Gill, P. J., Silbert, C. K. & Silbert, J. E. (1986) *Biochemistry* **25**, 405–410.
28. Saunders, S. & Bernfield, M. (1988) *J. Cell Biol.* **106**, 423–430.
29. Yamada, K. M. (1983) *Annu. Rev. Biochem.* **52**, 761–799.
30. Homandberg, G. A. (1987) *Biopolymers* **26**, 2087–2098.
31. Hummel, J. P. & Dryer, W. J. (1962) *Biochim. Biophys. Acta* **63**, 530–532.
32. Horwitz, A., Duggan, K., Greggs, R., Decker, C. & Buck, C. (1985) *J. Cell Biol.* **101**, 2134–2144.
33. Lam, L. H., Silbert, J. E. & Rosenberg, R. D. (1976) *Biochem. Biophys. Res. Commun.* **69**, 570–577.
34. Walicke, P. A., Feige, J.-J. & Baird, A. (1989) *J. Biol. Chem.* **264**, 4120–4126.
35. Moscatelli, D. (1987) *J. Cell Physiol.* **131**, 123–130.
36. Lobb, R. R., Harber, J. W. & Fett, J. W. (1986) *Anal. Biochem.* **154**, 1–14.
37. Laterra, J., Ansbacher, R. & Culp, L. A. (1980) *Proc. Natl. Acad. Sci. USA* **77**, 6662–6666.

The Structure of Type IX Collagen*

(Received for publication, July 20, 1984)

Michel van der Rest^{†‡}, Richard Mayne[§], Yoshifumi Ninomiya^{||}, Nabil G. Seidah^{**},
Michel Chretien^{**}, and Bjorn Reino Olsen^{†‡‡}

From the ^{||}Department of Biochemistry, University of Medicine and Dentistry of New Jersey, Rutgers Medical School, Piscataway, New Jersey 08854, the [§]Genetics Unit, Shriners Hospital, Montreal, Canada H3G 1A6, the ^{||}Departments of Anatomy and Biochemistry, University of Alabama in Birmingham, Alabama 35294, and the ^{**}Clinical Research Institute of Montreal, Canada H2W 1R7

We present a detailed analysis both of tryptic peptides and amino-terminal sequences of the subunits of two collagenous fragments (HMW and LMW) previously isolated from pepsin extracts of chicken cartilage (Reese, C. A., and Mayne, R. (1981) *Biochemistry* 20, 5443-5448). This analysis and a comparison with the nucleotide sequence of the cDNA pYN1738 (Ninomiya, Y., and Olsen, B. R. (1984) *Proc. Natl. Acad. Sci. U. S. A.* 81, 3014-3018) shows that HMW and LMW are pepsin-resistant fragments of a unique collagen composed of molecules with three different polypeptide chains (α -chains). This collagen has been assigned the type number IX, and the α -chain encoded by pYN1738 has been given the designation $\alpha 1(\text{IX})$.

Type IX collagen contains three triple-helical domains and at least two sets of interchain disulfide bridges. At the amino and carboxyl ends are noncollagenous domains which do not appear to be homologous to amino and carboxyl propeptides of interstitial collagens.

Recently we (1, 2) reported the synthesis and characterization of a clone, pYN1738, from a chick sternal cartilage cDNA library. Nucleotide sequencing of the insert of pYN1738 demonstrated that the sequence translates into a collagenous polypeptide with several unique characteristics. First, the polypeptides would contain three collagenous domains interspersed by short noncollagenous peptides. Second, several cysteinyl residues are located within the noncollagenous domains. These cysteinyl residues can potentially give rise to interchain disulfide bridges. Third, mRNA coding for the peptide is considerably smaller than mRNA encoding pro- α -chains of interstitial collagens. Based on a comparison between the characteristics of this polypeptide and properties of small collagenous protein fragments isolated from cartilage, we proposed (1, 2) that the pYN1738 insert codes for one of the three polypeptide chains of the parent molecule of the HMW and LMW collagenous fragments previously isolated from pepsin extracts of chicken cartilage (3, 4).

We now present a detailed analysis both of tryptic peptides

and amino-terminal sequences of the subunits of HMW and LMW, fractionated after reduction of interchain disulfide bridges. Based on this analysis and a comparison with the DNA sequences of pYN1738, we conclude that HMW and LMW are pepsin-resistant fragments of a unique collagen composed of molecules with three different polypeptide chains (α -chains). This collagen has been assigned the type number IX, and the α -chain encoded by pYN1738 has been given the designation $\alpha 1(\text{IX})$.

MATERIALS AND METHODS

Cloning and Nucleotide Sequencing of cDNA—The isolation of mRNA from 17-day-old chick sternal cartilage and synthesis of cDNA has been described (6). The screening of recombinant clones and the characterization of the cDNA clone pYN1738 has been reported (1). Nucleotide sequence analysis was performed by the method of Maxam and Gilbert (7).

Isolation and Fractionation of HMW and LMW—Collagens were solubilized from chicken sterna by limited pepsin digestion and HMW together with LMW were prepared by fractional salt precipitation as described previously (3). Isolation of the C2 component of HMW was accomplished by molecular sieve chromatography after reduction and alkylation of HMW (3, 4). Reduction and alkylation of LMW and separation of the three components LMW 1, LMW 2, and LMW 3 was as described (5).

Cleavage of Peptides with Trypsin—The peptides were dissolved in 0.2 M $(\text{NH}_4)\text{HCO}_3$ at a concentration of 1 mg/ml. Trypsin (Worthington) dissolved in water (1 mg/ml) was added to give an enzyme:substrate ratio of 1:30. After digestion at 37 °C for 4 h, the reaction was terminated by addition of a drop of glacial acetic acid. The samples were then dried in a Speedvac concentrator (Savant).

HPLC—The peptides were fractionated as described previously (8). The instrument used was from Beckman and consisted of a Model 334 chromatograph, a Model 160 UV monitor equipped with a zinc lamp and a CR1B data system. The column was C18 Vydac TP 201 (4.6 × 250 mm) from the Separation Group and it was protected with a guard column filled with pellicular C18 phase (Waters).

Amino Acid Analyses—The samples were hydrolyzed in 6 M HCl, containing 0.05% β -mercaptoethanol, for 20 h under nitrogen. The analyses were performed on a Dionex D-500 amino acid analyzer as described previously (9). S-Carboxymethylcysteine was estimated by using the color factor measured for L-cystine. Tryptophan was not quantitated.

Amino Acid Sequence Analysis—The amino acid sequences were determined by automated Edman degradation in a Beckman 890C protein/peptide sequencer as previously described (10). The phenylthiohydantoins of the amino acids were identified by HPLC as described by Lazure et al. (11).

RESULTS

Strategy for Determination of the Nucleotide Sequence of the cDNA pYN1738—As reported previously (1, 2) the nucleotide sequence of the 3200-base pair insert of pYN1738

* This investigation was supported by research Grants AM 21471 and AM 30481 from the National Institutes of Health of the United States Public Health Service, by Grant MA 7796 from the Medical Research Council of Canada, and by the Shriners of North America. The costs of publication of this article were defrayed in part by the payment of page charges. This article must therefore be hereby marked "advertisement" in accordance with 18 U.S.C. Section 1734 solely to indicate this fact.

§ A Chercheur Boursier from the Fonds de Recherche en Sante du Quebec.

†‡ To whom correspondence should be addressed.

¹ The abbreviation used is: HPLC, high-performance liquid chromatography.

shows that the coding strand of the cDNA contains about 150 adenylic acid residues at the 3' end preceded by about 100 nucleotides in the 3' nontranslated sequence between the first in-phase translational stop codon and the poly(A) tail. To determine the complete nucleotide sequence, restriction fragments were labeled using polynucleotide kinase and sequenced using the chemical cleavage method of Maxam and Gilbert (7). The strategy employed in cleaving the DNA with restriction endonucleases before end-labeling and the direction in which sequences were determined from different sites are shown in Fig. 1. As demonstrated in Fig. 1 almost all the nucleotide sequences have been determined by reading sequence gels of both strands.

Comparison between the Nucleotide Sequence of pYN1738 and Amino Acid Compositions of Tryptic Peptides Derived

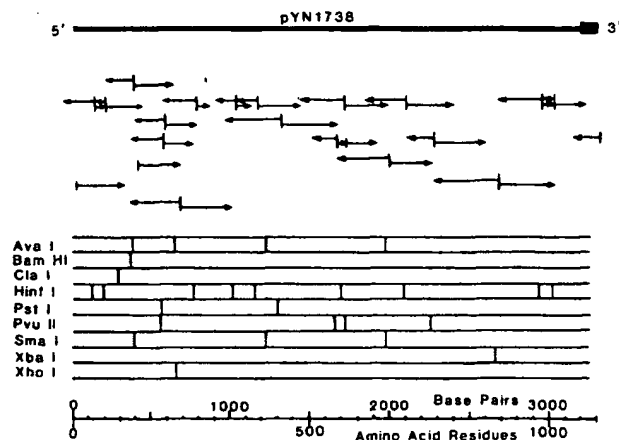


FIG. 1. Restriction endonuclease map of the pYN1738 cDNA insert. The strategy of nucleotide sequencing is indicated with vertical bars representing the position of 5' end labeling and the arrows showing the direction and length of the sequence analysis. On the basis of the DNA sequence analysis, the +1 coordinate was assigned to the first nucleotide at the 5' end of the insert. At the bottom of the figure the nucleotide/amino acid coordinates are indicated.

from LMW—Based on the presence of three collagenous domains and several cysteinyl residues within the polypeptide chain encoded by the pYN1738 insert, we proposed (1, 2) that this polypeptide represents one of the chains of a collagen that gives rise to HMW and LMW collagenous fragments during pepsin extraction of chicken hyaline cartilage. Support for this hypothesis also came from the close agreement between the molecular weights of the three collagenous domains as predicted from the number of amino acid residues and the molecular weights of HMW and LMW. To now provide definitive evidence for this identification, we separated the three different polypeptide subunits of LMW (LMW 1, LMW 2, LMW 3) by Cm-cellulose chromatography as described (5). Each of the subunits were digested with trypsin and the tryptic peptides were separated by HPLC. The amino acid compositions of the peptides were determined and compared with those predicted for tryptic fragments of the polypeptide chain encoded by pYN1738. This comparison clearly demonstrates that all the tryptic peptides recovered from LMW 3 can be found within the DNA-derived sequence. In contrast, none of the peptides recovered from the components LMW 1 and LMW 2 correspond to peptides predicted from the DNA sequence. Table I shows the amino acid compositions of the tryptic peptides of LMW 3 which could be separated by HPLC and the compositions predicted from the DNA sequence. The peptides are labeled according to their elution time (in minutes) from the HPLC column. The order in which the peptide compositions in Table I are arranged follows the sequence in which the peptides occur along the predicted sequence (Fig. 2). As shown in Table I, peptide 62 contains two internal arginyl residues. As can be seen from the sequence of Fig. 2 this must result from the known resistance of arginyl-prolyl peptide bonds to tryptic cleavage (12). A similar resistance has been noted for lysyl-hydroxyprolyl bonds (13). This explains why peptide 37 contains an internal lysyl residue. Peptides 19 and 54 both contain internal hydroxylysyl residues. We believe that the bonds at these residues may be resistant to trypsin because of O-glycosylation of the hydroxylysyl residues (13). Two of the peptide fractions from the HPLC analysis of LMW 3, fractions 6 and 5, are breakthrough

TABLE I
Amino acid compositions of tryptic peptides isolated from LMW 3

Peptide fraction	17	62	54	19	27	30	37	13	56	10
Cys(Cm)			0.4						1.4 (2)	
Hyp		5.9 ^a	2.0		1.0	1.0	2.7		3.6	
Asp + Asn		1.1 (1)						1.1 (1)		
Thr										
Ser	1.0 (1) ^b	0.5	0.5				1.0 (1)		1.4 (2)	
Glu + Gln		3.2 (3)	1.4 (1)	1.9 (2)			1.1 (1)		2.0 (2)	2.2 (2)
Pro		3.8 (11)	1.7 (3)	0.8 (1)	(1)	1.0 (2)	(3)		4.5 (11)	
Gly		10.1 (10)	5.9 (5)	3.0 (3)	2.3 (2)	2.4 (2)	4.3 (4)	1.3 (1)	7.9 (8)	2.1 (1)
Ala		2.0 (2)		0.9 (1)					1.0 (1)	0.9 (1)
Val								0.9 (1)	0.8 (1)	
Met										0.5 (1)
Ile			0.9 (1)						0.8 (1)	
Leu	1.0 (1)	2.0 (2)	1.6 (2)			1.0 (1)	1.0 (1)			
Tyr							0.9 (1)		0.8 (1)	
Phe		1.9 (2)			1.0 (1)					
His										
Hyl			0.7 ^a	1.6						
Lys			(1)	(2)			0.8 (1)			
Arg	1.0 (1)	3.0 (3)	1.0 (1)	1.0 (1)	1.0 (1)	1.0 (1)	1.0 (1)	1.0 (1)	1.0 (1)	1.0 (1)

^a Note that hydroxyprolyl and hydroxylysyl residues are found as prolyl and lysyl residues in the predicted sequence.

^b Values in parentheses are calculated from the sequence predicted from pYN1738.

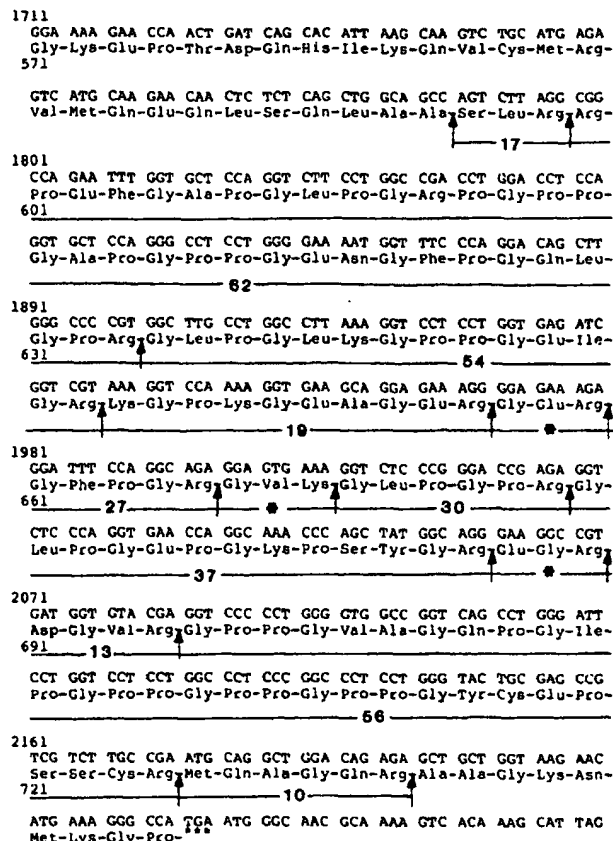


FIG. 2. Nucleotide/amino acid sequence of part of the $\alpha 1(\text{IX})$ mRNA/chain. Numbers above the nucleotide sequence represent coordinates as defined in the legend of Fig. 1; numbers below the amino acid sequence define the coordinates of the corresponding amino acid residues. The amino acid sequence includes the last three residues of the COL 2 domain, all the residues of the NC 2 domain, and the residues of the COL 1 and NC 1 domains. Different tryptic peptides isolated from LMW 3 by HPLC are indicated by numbers

below the amino acid sequence. Note the three tripeptides indicated by a star below the amino acid sequence. As discussed in the text these three peptides probably represent fraction 6 from the HPLC column. The vertical arrow at the left-hand side of peptide 17 indicates a peptide bond cleaved by pepsin. The remaining vertical arrows below the amino acid sequence indicate peptide bonds cleaved by trypsin.

fractions of the HPLC column, and they are not included in Table I. From amino acid analysis, the composition of fraction 6 is attributed to a mixture of the three starred tripeptides indicated in Fig. 2. Fraction 5 contains methionine, and the amino acid composition suggests that the fraction contains part of peptide 10 (see Fig. 2) in addition to a contamination by fraction 6. Since peptide 10 is localized close to the carboxyl-terminal end of the sequence deduced from pYN1738, the composition of the material in fraction 5 indicates that partial cleavage by pepsin occurs within peptide 10.

Amino-terminal amino acid sequence analysis of the LMW 3 component by automated Edman degradation provided definitive proof that LMW 3 is encoded by pYN1738. The analysis allowed identification of an amino acid sequence through 20 degradation cycles. A minor sequence identical to the major sequence but shifted one cycle could also be deduced from the analysis. As indicated in Fig. 3 the major and minor sequences result from the cleavage at two different sites by pepsin during the extraction of LMW collagen from cartilage.

Identification of Three Different Polypeptide Chains in HMW—It was previously reported that HMW collagen could be resolved into several components (C1, C2, C3, and C4) by Cm-cellulose chromatography (3, 4). In addition, electron microscopical studies of HMW using rotary shadowing showed that it consists of rod-like molecules with a short and a long arm and a kink between the arms. The data suggest that the C3 and C4 components are derived from the same polypeptide chain, that C3 and C4 are located within the long and short arms of HMW, respectively, and that the C2 component contains the other two polypeptide chains of HMW

AMINO-TERMINAL SEQUENCE ANALYSIS OF LMW 3

	595	600	605	610	615
pYN 1738	-Leu-Ala-Ala-Ser-Leu-Arg-Arg-Pro-Gln-Phe-Gly-Ala-Pro-Gly-Leu-Pro-Gly-Arg-Pro-Gly-Pro-Pro-Gly-Ala-Pro-				
LMW 3 (Major)	Ser-Leu-Arg-Arg-Pro-Gln-Phe-Gly-Ala-Hyp-Gly-Leu-Hyp-Gly-Arg-Hyp-Gly-Pro-Hyp-Gly-				
LMW 3 (Minor)	Leu-Arg-Arg-Pro-Gln-Phe-Gly-Ala-Hyp-Gly-Leu-Hyp-Gly-Arg-Hyp-Gly-Pro-Hyp-Gly-				

AMINO-TERMINAL SEQUENCE ANALYSIS OF THE C2 COMPONENT OF HMW

	80	85	90
pYN 1738	-Arg-Ile-Ser-Gln-Thr-Val-Ile-Glu-Arg-Gly-Leu-Pro-Gly-Pro-Pro-		
C2	Thr-Val-Ile-Glu-Arg-Gly-Leu-Hyp-Gly-Pro-Hyp-		

FIG. 3. Amino acid sequence analysis of LMW 3 (top) and of HMW C2 (bottom). The corresponding sequence for the peptide encoded by pYN1738 is given above each sequence. LMW 3 contained more than one sequence. These sequences were shown to correspond to different pepsin cleavage sites of the same peptide. Original data for sequencing runs will be made available on request.

(4). Whether the C2 component represents a single polypeptide sequence or a mixture of different, but closely related polypeptides, could not be determined in the earlier studies (3, 4).

When the reduced and alkylated C2 component was subjected to reverse-phase HPLC it could be separated into two peaks of identical areas (Fig. 4). As demonstrated in Fig. 5, the patterns of tryptic peptides derived from the two peaks differ from each other, as well as from those obtained for the components C3 and C4. The material in each of these peaks (for convenience now designated C2 and C5 in the description and discussion below) was then characterized further by tryptic peptide mapping using HPLC.

Comparison between the Nucleotide Sequence of pYN1738 and Amino Acid Compositions of Peptide Fragments Derived from HMW—Tryptic peptides isolated from the components C2, C3, C4, and C5 (see above) by HPLC were subjected to amino acid analysis. Amino acid analysis of all the peaks showed that not all the peaks in the chromatograms (Fig. 5) represented pure peptides. However, as shown in Table II, 7 peptide compositions from the C2 component of HMW could

be matched with the DNA-derived compositions. In contrast, no peptides recovered from C3, C4, or C5 matched the DNA-derived compositions.

Definitive proof that the C2 component of HMW is encoded by the cDNA pYN1738 was obtained from the amino-terminal amino acid sequence of C2. The result of this analysis is shown in Fig. 3. The amino acid sequence determined for C2 is clearly identical with the sequence deduced from the nucleotide sequence of pYN1738 (with the exception of post-translational hydroxylation of prolyl residues).

DISCUSSION

Type IX Collagen Contains Three Different Polypeptide Chains—As reported previously (5), analysis of tryptic peptide maps of subunits isolated from LMW after reduction and alkylation suggests that LMW contains three different polypeptide chains. From the analysis of tryptic peptides derived from the C2, C3, C4, and C5 components of HMW, reported in the present study, we conclude that each of the two triple-helical domains within HMW contains three different polypeptide subunits also. Type IX collagen, therefore, must contain three genetically distinct α -chains. One of these chains, $\alpha 1(\text{IX})$, contains amino acid sequences of the C2 component of HMW and of the LMW 3 subunit, and it is encoded by the cDNA pYN1738.

LMW is disulfide-bonded and migrates as a single component on polyacrylamide gel electrophoresis without reduction (5). Furthermore, chromatography of denatured, but nonreduced LMW on Cm-cellulose gives a single peak. Analysis of material from different fractions within this peak shows that the subunit composition of LMW is constant across the peak (5). We assume, therefore, that Type IX collagen molecules are heterotrimers of chain composition $\alpha 1(\text{IX}), \alpha 2(\text{IX}), \alpha 3(\text{IX})$. This is the most likely structure, but the available data do not rule out the possibility of a mixture of trimers with different chains.

Type IX Collagen Contains Three Triple-helical Domains—The three domains, previously called COL 1, COL 2, and COL 3 (1, 2), are separated by noncollagenous sequences (Fig. 6). Based on the amino acid sequence deduced from the nucleotide sequence of pYN1738, the lengths of the three domains are 137, 339, and 115 amino acid residues, respectively (1). It should be noted that because both the COL 1 and COL 3 domains contain imperfections in the Gly-X-Y triplet structure (1), the number of amino acid residues within these two domains are not multiples of three. The comparison between

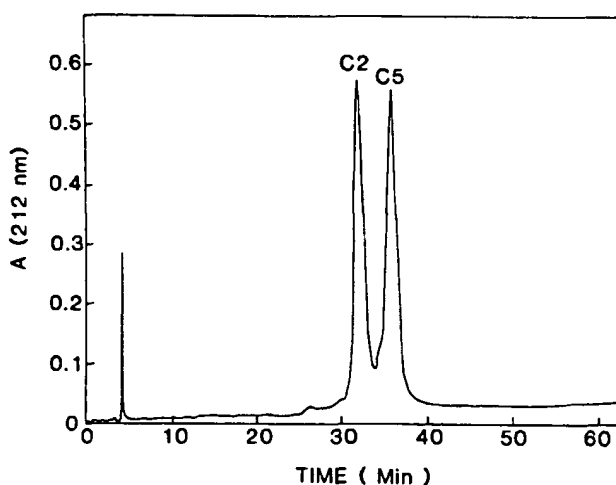
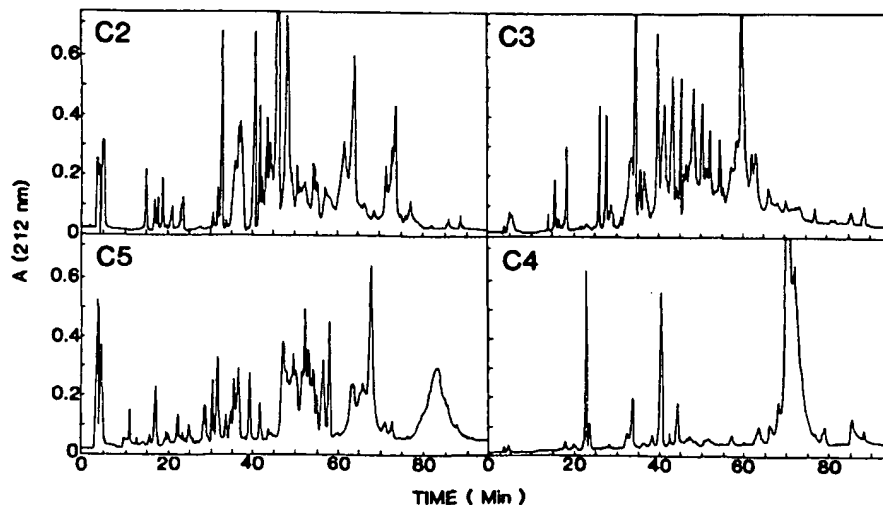


FIG. 4. Separation by HPLC of 170 μg of the C2 (original nomenclature) component of reduced and alkylated HMW (3) into fragments C2 and C5. The separation was done in the presence of 9 mM trifluoroacetic acid (1 g/liter) with an aqueous acetonitrile gradient (12.8–44.8%) over 60 min at room temperature. The flow rate was 1 ml/min.

FIG. 5. HPLC peptide maps of the tryptic peptides of HMW fragments C2, C3, C4, and C5. The separations were done in the presence of 9 mM trifluoroacetic acid (1 g/liter) with an aqueous gradient of acetonitrile (0–32%) over 90 min at room temperature. The flow rate was 1 ml/min. One-ml fractions were collected.



HMW collagen probably involve the two cysteinyl residues in the noncollagenous sequence NC 3. Involvement of these two cysteinyl residues in interchain disulfide bonds may explain why the 12-residue sequence of NC 3 in the $\alpha 1(\text{IX})$ chain is resistant to pepsin cleavage.

Our data do not exclude the possibility that the cysteinyl residue found within NC 2 also is part of HMW. This is because we have not located the tryptic peptide at the carboxyl end of the C2 component of HMW. Therefore, we do not know precisely where pepsin cleaves within the noncollagenous region NC 2 during pepsin extraction of cartilage (Fig. 6).

Noncollagenous Terminal Domains in Type IX Collagen Are Not Homologous to Amino and Carboxyl Properties of Interstitial Procollagens—The biosynthetic precursors of Type I, II, and III collagens are procollagens with large amino and carboxyl noncollagenous domains. For example, pro- $\alpha 1(\text{I})$ chains in Type I procollagen contains an amino propeptide of 139 residues and a carboxyl propeptide of 246 amino acid residues (for review, see Ref. 18). The amino acid sequence of the $\alpha 1(\text{IX})$ chain as deduced from the cDNA clearly shows that the terminal noncollagenous domains within the $\alpha 1(\text{IX})$ chain are unrelated to the sequence of such propeptides. The carboxyl-terminal noncollagenous domain (NC 1) in $\alpha 1(\text{IX})$ contains only 21 amino acid residues. The amino-terminal, noncollagenous domain (NC 4) of $\alpha 1(\text{IX})$ contains three cysteinyl residues within 85 amino acid residues as defined by the nucleotide sequence of pYN1738. However, since the open reading frame extends to the 5' end of the cDNA insert we cannot exclude the possibility that NC4 may even be longer than 85 amino acid residues. The amino acid sequence of NC 4 is clearly different from that of amino propeptides of Type I, II, and III procollagens.

Biosynthesis and Processing of Type IX Collagen—The size of the $\alpha 1(\text{IX})$ chain as described here is in agreement with estimated molecular weights for subunits of p-HMW and pM collagens, precursor molecules isolated from chick embryo sternal organ cultures (19, 20). We believe therefore that although the sequence deduced from pYN1738 may not include the complete amino-terminal region of $\alpha 1(\text{IX})$ chains (see above), the difference between the intact precursor chain and the available sequence is probably quite small.

Whether Type IX collagen is proteolytically processed to a smaller form during biosynthesis in cartilage is not known. If such processing does occur during the maturation of the protein, it probably involves the amino-terminal noncollagenous domain only. As noted above, the NC 1 domain of $\alpha 1(\text{IX})$ chains contains 21 amino acid residues of which 12 are found

in pepsin-solubilized LMW. This suggests that little, if any, processing occurs at the carboxyl end of the molecule. Pepsin-extracted HMW contains a nick between the C3 and C4 components in one of the three chains of the triple-helical molecule (4), and it is possible that this nick is not due to the treatment with pepsin, but is the result of some processing step during biosynthesis of Type IX collagen.

Acknowledgments—We wish to thank E. Rodriguez and E. Wan for technical assistance.

REFERENCES

1. Ninomiya, Y., and Olsen, B. R. (1984) *Proc. Natl. Acad. Sci. U. S. A.* **81**, 3014–3018
2. Ninomiya, Y., Showalter, A. M., and Olsen, B. R. (1984) in *The Role of Extracellular Matrix in Development* (Trelstad, R. L., ed) pp. 255–275, Alan R. Liss, Inc., New York
3. Reese, C. A., and Mayne, R. (1981) *Biochemistry* **20**, 5443–5448
4. Reese, C. A., Wiedemann, H., Kuhn, K., and Mayne, R. (1982) *Biochemistry* **21**, 826–830
5. Mayne, R., van der Rest, M., Weaver, D. C., and Butler, W. T. (1984) *J. Cell. Biochem.*, in press
6. Ninomiya, Y., Showalter, A. M., van der Rest, M., Seidah, N. G., Chretien, M., and Olsen, B. R. (1984) *Biochemistry* **23**, 617–624
7. Maxam, A., and Gilbert, W. (1980) *Methods Enzymol.* **65**, 499–560
8. van der Rest, M., and Fietzek, P. P. (1982) *Eur. J. Biochem.* **125**, 491–496
9. van der Rest, M., Cole, W. G., and Glorieux, F. H. (1977) *Biochem. J.* **161**, 527–534
10. Seidah, N. G., Rochemont, J., Hamelin, J., Lis, M., and Chretien, M. (1981) *J. Biol. Chem.* **256**, 7977–7984
11. Lazure, C., Seidah, N. G., Chretien, M., Lallier, R., and St-Pierre, S. (1983) *Can. J. Biochem.* **61**, 287–292
12. Keil, B. (1982) in *Methods in Protein Sequence Analysis* (Elzinga, M., ed) pp 291–304, Humana Press, Clifton, NJ
13. Fietzek, P. P., Allman, H., Rauterberg, J., Henkel, W., Wachter, E., and Kuhn, K. (1979) *Hoppe-Seyler's Z. Physiol. Chem.* **360**, 809–820
14. Schuppan, D., Glanville, R. W., and Timpl, R. (1982) *Eur. J. Biochem.* **123**, 505–512
15. Benya, P. D. (1980) *Renal Physiol.* **3**, 30–35
16. Sage, H., Trueb, B., and Bornstein, P. (1983) *J. Biol. Chem.* **258**, 13391–13401
17. Bentz, H., Morris, N. P., Murray, L. W., Sakai, L. Y., Hollister, D. W., and Burgeson, R. E. (1983) *Proc. Natl. Acad. Sci. U. S. A.* **80**, 3168–3172
18. Bornstein, P., and Sage, H. (1980) *Annu. Rev. Biochem.* **49**, 957–1003
19. Bruckner, P., Mayne, R., and Tuderman, L. (1983) *Eur. J. Biochem.* **136**, 333–339
20. von der Mark, K., van Menzel, M., and Wiedemann, H. (1984) *Eur. J. Biochem.* **138**, 629–633